Properties of systems with time delayed feedback

Dissertation
zur Erlangung des Doktorgrades
der Fakultät der Naturwissenschaften (Dr. rer. nat.)
der Bergischen Universität Gesamthochschule Wuppertal
WUB-DIS 2002-4

vorgelegt von
Elisangela Ferretti Manffra
aus Curitiba
Februar 2002

Abstract

Nonlinear dynamics is a vast field complementary to classical mechanics and statistical physics. Inside this field we have chosen to study dynamical systems with time delayed feedback. Such systems appear as models in the sciences like physics, biology, economy and have at the same time interesting theoretical properties being good candidates to present high dimensional attractors. In this work delayed systems are studied mainly in the limit of large delay were the scaling properties of the attractors are observed. In chapter 2 we describe general properties of periodic orbits of dynamical systems with feedback delay. In chapter 3 it is shown that the marginal invariant density of chaotic attractors of scalar systems with time delayed feedback has an asymptotic form in the limit of large delay. We present general considerations, detailed analytical results in low order perturbation theory for a particular model, and numerics for the understanding of the asymptotic behaviour of the projections of the invariant density. Our approach clarifies how the analytical properties of the model determine the behaviour of the marginal invariant densities for large delay times. In chapter 4 properties of the topological and metric entropies are discussed and arguments for the boundedness of both are given on the basis of periodic orbits and of the asymptotic behavior of the invariant density. In chapter 5 we analyse the representation of maps with time delayed feedback as coupled map lattices. We show that when the delayed map has an anomalous exponent, this representation gives rise to infinitely large comoving Lyapunov exponents of the spatially extended system. Additionally, we present a short discussion regarding the anomalous error propagation in the case of continuous time, i.e. delayed differential equations.

Contents

List of Figures

List of Tables

Chapter 1

Introduction

Nonlinear dynamics is a fascinating research field due to the scope of problems that can be treated with theoretical concepts and tools related to it. The theory of dynamical systems dates back to the end of the 19th century with the problems like the three body, the ergodic hypothesis and nonlinear oscillators. These three problems brought the necessity of a theoretical framework complementary to classical mechanics and statistical physics. During the last 40 years there have been considerable developments in this field motivated by numerical and real experiments showing complex motion. It is possible to say that the field of dynamical systems has been growing in the interface between sciences (e.g. physics, chemistry, geology, physiology, biology, ecology, engineering, economy) and mathematics. Nowadays one counts with a consistent theoretical framework which combines statistical and geometrical/topological concepts providing a variety of tools to describe and understand the irregular motion and the complex patterns observed in nonlinear systems in numerical and real experiments.

Inside this vast universe, we have decided to study a special class of nonlinear dynamical systems: systems with a delayed feedback. The dynamics of these systems depends not only on the present but also on the past values of the dynamical variables. They appear as models for control process in a variety of fields. Moreover, these systems present interesting scaling properties at large delay: The dimension of attractors may scale linearly with the delay value while the entropy remains bounded. In this work we treat some issues related to systems with time delayed feedback. Before we enter in this subject some definitions about dynamical systems in general are discussed in the next section.

1.1 Dynamical systems and nonlinear phenomena

Differential equations of the form

$$\dot{x}(t) = \mathbf{F}_\mu(x(t)) \qquad x \in \mathbb{R}^d \tag{1.1}$$

which induce the mapping $x(t) = \Phi^t_\mu(x(0))$ in $\mathbb{R}^d$ are called dynamical systems. Here $x(0)$ is the initial condition and μ is some parameter or set of parameters. The mapping produces unique solutions on a set A i.e. the solutions depend uniquely on $x(0)$ under general conditions for $F_\mu(x)$ (Lipshitz condition in A, see e.g. [3]).

$F_\mu(x)$ may have solutions of a simple form like diverging to infinity, fixed points, periodic points and coexistence of such solutions. If the map is volume contracting than the solutions may converge to a compact set called attractor which might be a fixed point, a periodic orbit or a more complex set like homoclinic orbits or a chaotic attractor. When fixed points and periodic orbits are considered, a local theory can be developed and bifurcations of these solutions might be studied as in [4]. For the characterisation of chaotic attractors statistical aspects such as the invariant density, Lyapunov exponents and entropies [5, 1] must be taken into account.

1.2 Dynamical systems with delayed feedback

There are situations in which some additional dependence on the past states is required, i.e. some memory must be taken into account. Such models appear in physiology [6, 7], biology [8], laser physics (see e.g. [9, 10, 11, 12]), economy [13], and other examples that can be found in [14]. One example is the so-called Mackey-Glass [6] equation constructed to model the production of red blood cells

$$\dot{x} = -bx(t) + \frac{ax(t-\tau)}{(1 + x(t-\tau)^{10})} \tag{1.2}$$

All these models can be classified as belonging to a special class of differential equations, the so called [14] differential difference equations (DDE):

$$\dot{x}(t) = F(x(t), x(t-\tau)) \tag{1.3}$$

where $x \in R^d$. More generally, one may also consider the case of several delay values. The solutions of Eq.(1.3) are unique when a function $\phi(t)$ with $t \in [-\tau, 0]$ is specified as initial condition. Therefore $\Phi^t_\mu(\phi)$ is a mapping from the space of functions into this space, and the solutions of Eq. (1.3)

live on a phase space that is infinite dimensional. As a consequence, Eq. (1.3) may have attractors of arbitrary high dimension being one of the possible prototypes for high dimensional chaos. A detailed description of the mathematical properties of Eq. (1.3) is given in [14].

A discretized version of Eq.(1.3) gives what is called in [14] a difference equation and we call in this work delayed map:

$$x_{n+1} = F(x_n, x_{n-T}) \tag{1.4}$$

with $x \in \mathbb{R}^d$ in general but we restrict here to the case $x \in \mathbb{R}^1$ which shows the phenomenology we are interested in. Eq. (1.4) can be written in a vectorial variable $\mathbf{x}$ with components $x^{(i)} = x_{n-i}$:

$$\begin{aligned} x_{n+1}^{(0)} &= F(x_n^{(1)}, x_n^{(T)}) \\ x_{n+1}^{(i)} &= x_n^{(i-1)} \qquad , 1 \leqslant i \leqslant T \end{aligned} \tag{1.5}$$

i.e. we have a map

$$\mathbf{x}_{n+1} = \mathbf{G}(\mathbf{x}_n). \tag{1.6}$$

with $\mathbf{x} \in \mathbb{R}^{T+1}$, i.e. changing the delay value we change the dimensionality of the phase space. Important properties of these maps will be discussed in this work. Unfortunately, delayed maps and delayed differential equations cannot be related to each other using the technique of Poincarè surface section as in ordinary differential equations [1]. A relation between delayed maps and delayed differential equations does not exist formally, but it is possible to observe that they share essentially all properties we are interested in.

1.2.1 Routes to chaos in delayed systems

A whole theory on linear delayed differential equations exist already for four decades (see e.g. [16, 3, 8]) and is essential in discussing the stability of fixed points. Such theory shows in a general way that the number of unstable directions increases as the delay increases, pointing out the mechanisms for increasing dimensionality of the solutions. Indeed, in many works about specific DDE's, authors make use of such a theory to discuss the Hopf bifurcation [6, 17, 15]: The way in which a stable fixed point loses stability as delay increases. Many works concentrate in the study of routes to chaos in their models of interest. A classical example is the laser system discussed

[1] There is a method proposed in [15] to obtain such surface section, but it does not reduce the dimensionality of the phase space

by Ikeda [9] where new odd harmonics appear as the delay increases, which are unstable and coexist in the limit of large delay when high dimensional chaotic solutions exist. Other examples report routes resembling period doubling cascades with hysteresis (coexistence of attractors), boundary crisis [18], or appearance and breakdown of tori and intermittency [10]. More generally, bifurcations of solutions of these equations were discussed in [15]. Some works, where an analytical treatment is accomplished are restricted to delay values near a Hopf bifurcation where some reduction to the central manifold can be performed and the delayed equation can be approximated by an ODE (see [17] for an example applied to enzyme dynamics and [19] for a more general formulation). At large delay the same techniques applied to spatially extended systems might be used to treat the problem of bifurcations of fixed points [11, 12].

1.2.2 Asymptotic behavior of attractors

When chaotic behavior is observed, it is typical that changing the delay value changes the dimension of attractors. High dimensional attractors are observed numerically in [20, 9, 21, 22]. The Lyapunov exponents and the estimations of the dimension and entropy based on them show that these attractors have an asymptotic behavior for delay values large enough as illustrated in figure 1.1 and 1.2 for a specific example.

Although the technique of the Poincaré surface of section does not yield, in general, a direct relationship between delayed maps and delayed differential equations, Eqs. (1.3) and (1.4), attractors of time continuous and time discrete delayed systems share the same asymptotic properties (figures 1.1 and 1.2 are obtained for a delayed map while in references [20, 9, 21, 22] delayed differential equations are considered). This is the reason why in chapters 3 and 4 only delayed maps are studied in detail.

1.3 Outline of the work

In this work four issues related to delayed systems are treated in detail. In chapter 2 periodic orbits of Eq.(1.4) and Eq.(1.3) are discussed. Chapters 3 and 4 are devoted to the study of asymptotic properties of attractors in the large delay limit. In chapter 3 the scalar induced invariant density is discussed, namely it is observed numerically that an asymptotic form of this density exists and for an specific map its analytical form is derived using perturbation treatment of the Frobenius-Perron operator. In chapter

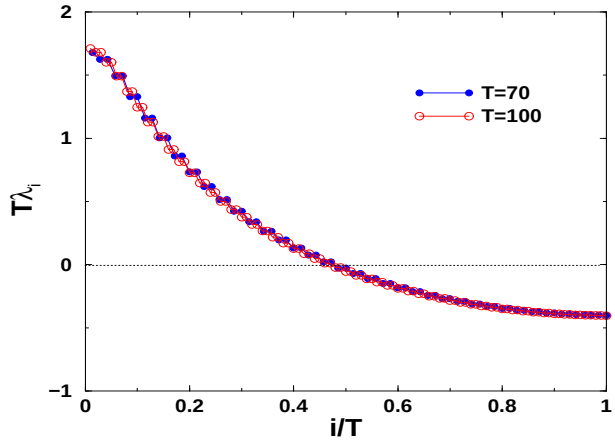

Figure 1.1: Spectrum of Lyapunov exponents for the delayed Hénon map - Eq. (2.16) with $a = 1.0$, $b = 0.3$. The exponents are multiplied by T and its index is divided by the delay value in order to see the superposition of the spectra (there exist $T + 1$ exponents).

4 the asymptotic behavior of the entropy of the attractor is considered in an attempt to explain the mechanisms responsible for the asymptotic behavior depicted in figure 1.2 beside the behaviour of the spectrum of Lyapunov exponents. Chapter 5 treats the comoving Lyapunv exponents in coupled map lattices derived from delayed maps, and hence is related to the relevant issue of a spatial representation of DDE's.

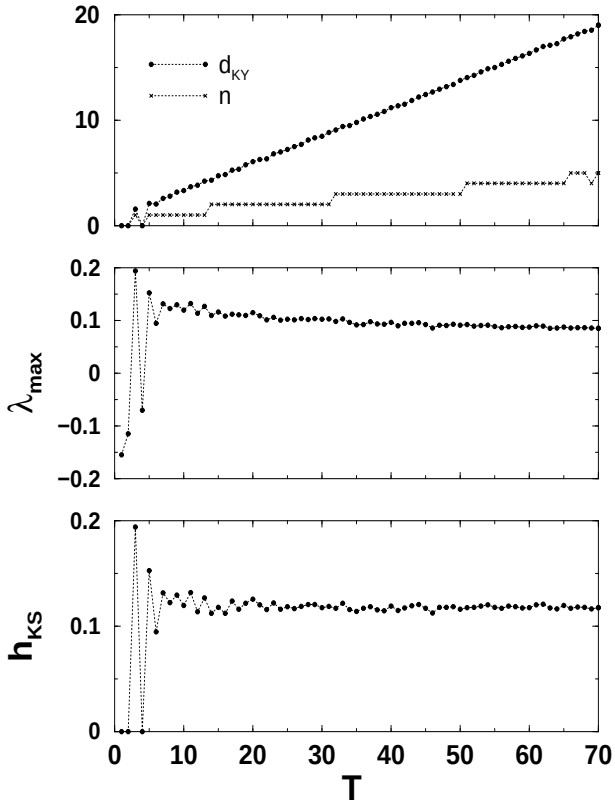

Figure 1.2: Upper panel: Dependence of the Kaplan-Yorke dimension d_{KY} and the number of unstable Lyapunov exponents on the delay T for the map (2.16) with $a = 1.0$, $b = 0.3$. Middle and lower panel: maximal Lyapunov exponent λ_{max} and Kolmogorov-Sinai entropy h_{KS} estimated with Pesin's identity [1].

Chapter 2

Periodic orbits

2.1 Why studying periodic solutions?

Studying the fixed points, periodic orbits and their stability is usually in dynamical systems theory the first step to understand the structure of the manifolds where solutions of such system exist. Through the so called bifurcation theory [4, 23] one can analyse how existence and stability of these regular solutions are affected as parameters change and at which parameter values important qualitative changes happen (i.e. solutions are created or disappear; there are dramatic changes in their stability). One may observe for instance a route to chaos through a period doubling cascade, breaking tori, crisis or other forms classified in the literature [5].

Additionally, when chaotic solutions are present, they coexist with a set of unstable periodic orbits which is dense in the manifold where such solutions live. Having this statement as a basis, a whole theory was developed making use of unstable periodic orbits to construct an approximation of the invariant density [24, 25] and to obtain ergodic averages in a thermodynamic formulation of the theory of dynamical systems.

These two branches of nonlinear dynamics have motivated the study of periodic solutions of delayed systems and to investigate how their existence and stability are affected by changes in the delay value (the parameter we want to investigate). In this chapter we present some results about periodic orbits of delayed systems. We have tried to keep the treatment general and concentrate on how the set of periodic orbits and their stability change as the delay increases. First we have treated the case of delayed maps: Since their phase space is finite dimensional they behave like conventional maps

in this vectorial phase space. We have made use of the theory existent for conventional maps to study the orbits and their stability and employed a trick in order to make the bifurcation parameter - the delay - a continuous variable. The main results are presented in section 2.2. The orbits of DDE's are discussed in section 2.3 where we present a general result about the existence of orbits at different delay values.

2.2 Periodic solutions of delayed maps

We have decided to investigate periodic solutions of maps of the form Eq. (1.4). From these studies we cannot draw any conclusion about the delayed differential equations, but through it we have gained intuition that was useful in the continuous case. Furthermore, we derived a property about the orbits that will be useful in chapter 4 when we discuss the topological entropy of these maps.

2.2.1 Periodic orbits at different delays

The first result of this work concerns the existence of periodic orbits of Eq.(1.4) at different delay values. Let us first define a p-periodic orbit by a sequence of points

$$\{\overline{x}_0, \overline{x}_1, \overline{x}_2, ..., \overline{x}_{p-1}\} \tag{2.1}$$

(later called periodic points), which repeats in time as Eq.(1.4) is iterated. These points obey the equations:

$$\overline{x}_{i+1} = F(\overline{x}_i, \overline{x}_{i-T}) \tag{2.2}$$

for $0 \leqslant i \leqslant p-1$, with the boundary condition

$$\overline{x}_0 = F(\overline{x}_{p-1}, \overline{x}_{p-1-T}) \tag{2.3}$$

where the indices are understood modulo the period p.

Inspecting Eqs. (2.2) and (2.3) one can find the following property about the existence of periodic orbits at different delays: Eqs. (2.2), (2.3) are invariant under the transformation $T \mapsto T + np$, $n \in \mathbb{Z}$ of the delay value. Every period-p orbit found for a delay value T will be also a period-p orbit for $\tilde{T} = T + np$, as long as $\tilde{T}$ and T are both positive.

As a consequence, one has the following relation for the p-periodic points of the map:

$$N(p, T) = N(p, T + np), \tag{2.4}$$

where $N(p,T)$ denotes the number of p-periodic points for a delay T. Eqs.(2.2) and (2.3) can be also written for a map with $x \in \mathbb{R}^d$ and therefore the property about the orbit is also valid for such systems.

2.2.2 Stability of orbits at different delays

The stability properties of periodic orbits are studied analysing how small perturbations around the orbit, say $\delta\mathbf{x}_n$, evolve in time. Such evolution is given by the linearisation of the map around a point under consideration (map in the tangent space), i.e. the evolution equation of the perturbations is given by:

$$\delta\mathbf{x_{n+1}} = \mathbf{J}(\mathbf{x_n})\delta\mathbf{x_n} \tag{2.5}$$

where $\mathbf{J}(\mathbf{x_n}) = \frac{\partial\mathbf{F}(\mathbf{x_n})}{\partial\mathbf{x_n}}$ is the Jacobi matrix at the point $\mathbf{x}_n$, which in the case of Eq. (1.6) assumes the form:

$$\mathbf{J}(\mathbf{x}) = \begin{pmatrix} \frac{\partial F(x^{(0)},x^{(T)})}{\partial x^{(0)}} & 0 & \dots & 0 & \frac{\partial F(x^{(0)},x^{(T)})}{\partial x^{(T)}} \\ 1 & 0 & \dots & 0 & 0 \\ 0 & 1 & \dots & 0 & 0 \\ \ddots & & & & \\ 0 & 0 & \dots & 1 & 0 \end{pmatrix}. \tag{2.6}$$

In order to study the stability of a periodic orbit one has to study the evolution of the perturbation during a full period, i.e. how is $\delta\mathbf{x}_{n+p}$ as a function of $\delta\mathbf{x}_n$. From Eq.(2.5) one can see that:

$$\delta\mathbf{x_{n+p}} = [\prod_i \mathbf{J}(\overline{\mathbf{x}}_\mathbf{i})]\delta\mathbf{x}_n. \tag{2.7}$$

The eigenvalues μ_i of the matrix $\prod_i \mathbf{J}(\overline{\mathbf{x}}_\mathbf{i})$ are the characteristic multipliers, i.e. the roots of the characteristic equation

$$\det[\prod_{i=n}^{n+p-1} \mathbf{J}(\overline{\mathbf{x}}_\mathbf{i}) - \mu\mathbb{I}] = 0 \tag{2.8}$$

are associated with the Lyapunov exponents λ_i of the orbit defined by:

$$\lambda_i = \frac{1}{2p}\ln\mu_i^*\mu_i \tag{2.9}$$

ordered such that $\lambda_i \geqslant \lambda_{i+1}$. The orbit is stable if $\lambda_i \leqslant 0 \qquad \forall i$. Unstable orbits have one or more positive exponents and their number corresponds

to the dimension of the unstable manifold [23] - here denoted d_{um}- of the orbit.

Using the property that p–periodic orbits do not change if we increase the delay by $T \mapsto T+np$, one can study how the stability of the orbits change when the delay increases according to this rule. Of particular interest is the behaviour of the dimension of their unstable manifolds as the delay increases. Due to the form of the Jacobi matrix of delayed maps, the characteristic equation (2.8) is a polynomial equation of degree $T+1$. At large delays (more precisely if the delay is larger than the period) Eq. (2.8) assumes an asymptotic form whose coefficients depend on the periodic points, but not on the delay value T, while the exponents depend on the delay value. More explicitly, at large T Eq.(2.8) assumes the form:

$$g(\mu) = \mu^{T+1} + C_1\mu^{a_1T+b_1} + C_2\mu^{a_2T+b2} + ... + C_{p+1} = 0 \tag{2.10}$$

where C_i are coefficients that depend on the periodic points and a_i, b_i are constants (usually rational numbers).

With this knowledge, it is possible, for each orbit, to investigate how the spectrum of Lyapunov exponents changes as the delay increases. One can compute all the spectrum looking for the roots of Eq.(2.10) at different delays. Alternatively, one might obtain the dimension of the unstable manifold counting the number of roots of $g(\mu^{-1})$ within $|\mu^{-1}| < 1$. Using the same procedure as in [26], one can obtain the number of such roots counting the number of times the path traced by $g(\mu^{-1})$ winds around the origin as μ^{-1} is varied one full time around the unit circle. In the next paragraphs we discuss two examples of orbits and their corresponding characteristic equation to clarify these ideas.

First let us consider $p = 1$, i.e. the fixed point. Since the fixed points are not affected by the delay value, this is the simplest periodic solution one could investigate. The characteristic equation has the form:

$$\mu^{T+1} + C_1(\overline{x}_0)\mu^T + C_2(\overline{x}_0) = 0 \tag{2.11}$$

where we have defined: $C_1(\overline{x}_0) = \frac{\partial F(x,y)}{\partial x}|_{x=y=\overline{x}_0}$ and $C_2 = \frac{\partial F(x,y)}{\partial y}|_{x=y=\overline{x}_0}$. The fixed points are the same for all delay values T. Now it is possible to analyse the solutions of such an equation in different situations, for different conditions of C_1 and C_2, but a case of interest here is that of an unstable fixed point. As T increases the number of multipliers increases but for large delay their spectrum relaxes to an asymptotic form as discussed in [27] where most exponents scale like T^{-1}. The main argument for this asymptotic

behaviour is the following: since C_1 and C_2 are finite, if the multipliers are such that some $\mu > 1.0$ (unstable fixed point), these must obey the Ansatz $\mu \propto e^{1/T}$. It is possible also that one of the multipliers is independent of T (the anomalous exponent pointed out in [27]), and this happens in the cases when $C_2 << 1.0$ and $C_1 > 1.0$.

In order to have an idea of how Eq.(2.10) may look like in a more general case, let us consider a periodic orbit with $p = 3$, existent at $T = 3 + 3n$ with $n = 0, 1, 2, ...$ If a delayed map allows such orbit, the corresponding characteristic equation reads:

$$\mu^{(T+1)} - \mu^T C_1(\overline{x}_1, \overline{x}_2, \overline{x}_3) + \mu^{\frac{2T}{3}} C_2(\overline{x}_1, \overline{x}_2, \overline{x}_3) + \mu^{\frac{T}{3}} C_3(\overline{x}_1, \overline{x}_2, \overline{x}_3) + C_4(\overline{x}_1, \overline{x}_2, \overline{x}_3) = 0. \tag{2.12}$$

Here:

$$\begin{aligned} C_1(\overline{x}_1, \overline{x}_2, \overline{x}_3) &= \partial_1 F(\overline{x}_1, \overline{x}_1)\partial_1 F(\overline{x}_2, \overline{x}_2)\partial_1 F(\overline{x}_3, \overline{x}_3) \\ C_2(\overline{x}_1, \overline{x}_2, x_3) &= \partial_1 F(\overline{x}_2, \overline{x}_2)[\partial_1 F(\overline{x}_1, \overline{x}_1) + \\ &\partial_1 F(\overline{x}_3, \overline{x}_3)\partial_2 F(\overline{x}_1, \overline{x}_1) + \partial_1 F(\overline{x}_1, \overline{x}_1)\partial_2 F(\overline{x}_3, \overline{x}_3)] \\ C_3(\overline{x}_1, \overline{x}_2, \overline{x}_3) &= \partial_1 F(\overline{x}_3, \overline{x}_3)\partial_2 F(\overline{x}_1, \overline{x}_1)\partial_2 F(\overline{x}_2, \overline{x}_2) \\ &+\partial_2 F(\overline{x}_3, \overline{x}_3)[\partial_1 F(\overline{x}_2, \overline{x}_2)\partial_2 F(\overline{x}_1, \overline{x}_1) + \\ &\partial_1 F(\overline{x}_1, \overline{x}_1)\partial_2 F(\overline{x}_2, \overline{x}_2)] \\ C_4(\overline{x}_1, \overline{x}_2, \overline{x}_3) &= \partial_2 F(\overline{x}_1, \overline{x}_1)\partial_2 F(\overline{x}_2, \overline{x}_2)\partial_2 F(\overline{x}_3, \overline{x}_3) \end{aligned} \tag{2.13}$$

where we have defined $\partial_1 F = \frac{\partial F(x,y)}{\partial x}$ and $\partial_2 F = \frac{\partial F(x,y)}{\partial y}$, for convenience. This equation is valid at all delay values $T = 3 + 3n$, and each of its zeroes yields one of the $3 + 3n$ Lyapunov exponents of this orbit.

2.2.3 Bifurcation analysis

Besides the question of how many unstable directions one orbit has and how this number grows as the delay increases, one could ask which kind of bifurcations are associated with this growth. In other words, considering the delay value as parameter we ask which kind of bifurcation takes place as the delay value increases. Bifurcations are related to changes in topology

(appearance and disappearance of fixed points) or in the stability of periodic orbits.

This analysis would be very natural if the delay value were a real number which is not the case of delayed maps. We tackle this problem constructing another kind of map, where two delay values are involved (T_1 and $T_2 = T_1 + 1$) and which has a real parameter $\tau \in [0, 1]$ that controls the weight of each contribution:

$$x_{n+1} = f_1(x_n) + a_1(\tau) f_2(x_{n-T_1}) + a_2(\tau) f_2(x_{n-T_2}) \tag{2.14}$$

where:

$$a_{1/2}(\tau) = cos^2[\frac{\pi}{2}(\tau - T_{1/2})]. \tag{2.15}$$

We have chosen this function because it has the properties: $a_1(\tau) + a_2(\tau) = 1.0$ and we have only one delay value at $\tau = 0/1$, i.e. at these extrema values the map has only one of these two delays and corresponds to Eq. (1.4).

With this method, it is possible to see which kind of bifurcation takes place, but it has two disadvantages: First it is only possible to analyse delayed maps where the instantaneous and delayed contribution appear as a sum; second the type of bifurcation found might depend on the specific form of $a_{1/2}(\tau)$. In despite of these disadvantages, we apply this method in a specific example to be discussed in the following section.

2.2.4 The Hénon map with delay : an example

Let us consider now a special map in order to clarify all the ideas presented in the former sections, the version with time delay of the Hénon map:

$$x_{n+1} = a - x_n^2 + b x_{n-T} \tag{2.16}$$

which corresponds to usual the Hénon map if $T = 1$.

Stability of fixed points

There are two fixed points for the map (2.16):

$$\overline{x}_{+,-} = 0.5(b - 1 \pm \sqrt{(b-1)^2 - 4a}). \tag{2.17}$$

If $a > -0.25(1-b)^2$ the fixed points are real and we can study their stability and how it depends on a and b. In this case, the parameters of equation

(2.11) are $C_1 = 2\overline{x}_{+,-}$ and $C_2 = b$. The stability depends indirectly on the parameter a since it determines the value of the fixed point.

The asymptotic spectra at $T \to \infty$ of these two fixed points will be different, since the Jacobian of the map has not the same value. One interesting question to ask is if the spectra possess an anomalous exponent or not, and the condition for existence of such exponent is that $2\overline{x}_{+,-} > 1.0$. In words, this condition will divide the parameter plane $\{a, b\}$ into regions where one of the two fixed points will have an anomalous exponent, or both, or none of them.

We specify now the parameter values $a = 1.0$ and $b = 0.3$, such values that will be used in subsequent analysis when chaotic motion will be investigated. Investigating the stability of both fixed points as the delay increases, we obtain the results illustrated in figures 2.1 and 2.2. For these parameter values, both fixed points have an anomalous exponent at large delay. The corresponding spectra are shown in figure 2.2. As the delay increases new exponents become positive but their absolute value is reduced, this is true for the whole spectrum except the anomalous exponent. A closed form for these quasicontinuous part of the spectrum in the limit $T \to \infty$ can be found in [27].

Some periodic orbits with short period

Now we apply the ideas of sections 2.2.1 and 2.2.2 to study the periodic orbits of Eq. (2.16). First let us consider the period two orbits existent at $T = 2k + 2$. The corresponding characteristic equation reads:

$$\mu^{T+1} - 4\overline{x}_1\overline{x}_2\mu^T + 2b(\overline{x}_1 + \overline{x}_2)\mu^{T/2} - b^2 = 0 \tag{2.18}$$

with $T \geqslant 2$.

We obtain numerically the solutions of Eq. (2.18), and consequently the spectrum of Lyapunov exponents at different delay values. The maximal eigenvalue $\lambda_1 = \frac{1}{2}\log(|\mu_1|^2)$ is independent of the delay value at large delays as can be seen in figure 2.3, i.e. using the nomenclature of [27] one might say that this orbit has an anomalous exponent. The appearant discontinuity of the curve at delay $T = 38$ is related to a pair of complex eigenvalues that split giving rise to the anomalous eigenvalue. This orbit is stable for $T = 2$ and unstable for all other delay values.

An overview of how the spectrum depends on the delay can be seen in figure 2.4 where the dimension of the unstable manifold d_{um} and the

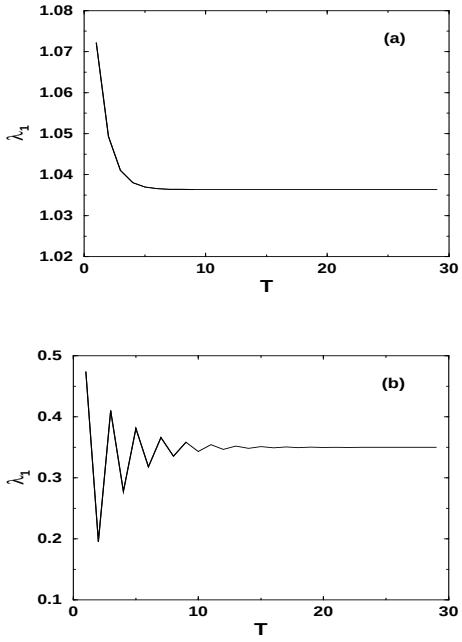

Figure 2.1: Maximal Lyapunov exponent of the fixed points of Hénon map with $a = 1.0$ and $b = 0.3$. (a) for $\overline{x}_+$ and (b) of $\overline{x}_-$.

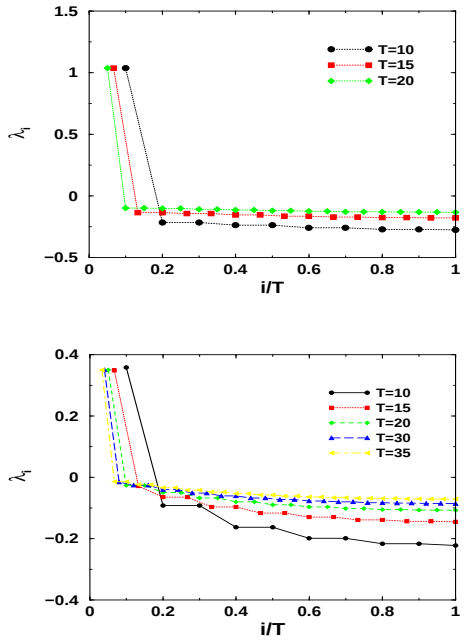

Figure 2.2: Spectrum of Lyapunov exponents of the fixed points of Hénon map with $a = 1.0$ and $b = 0.3$. (a) for $\overline{x}_+$ and (b) of $\overline{x}_-$.

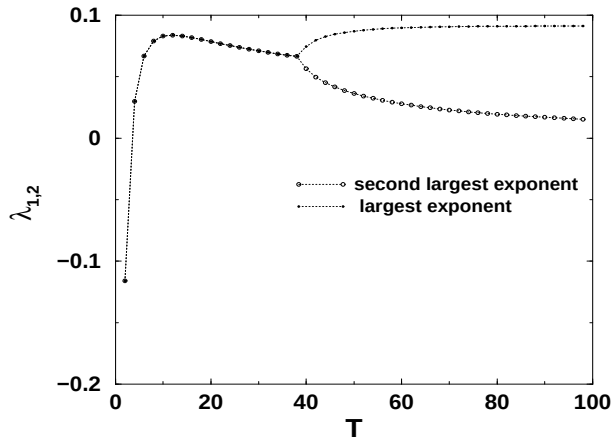

Figure 2.3: First and second maximal Lyapunov exponents of the period two orbit of (2.16) with $a = 1.0$ and $b = 0.3$ existent for $T = 2k + 2$ as a function of the delay value.

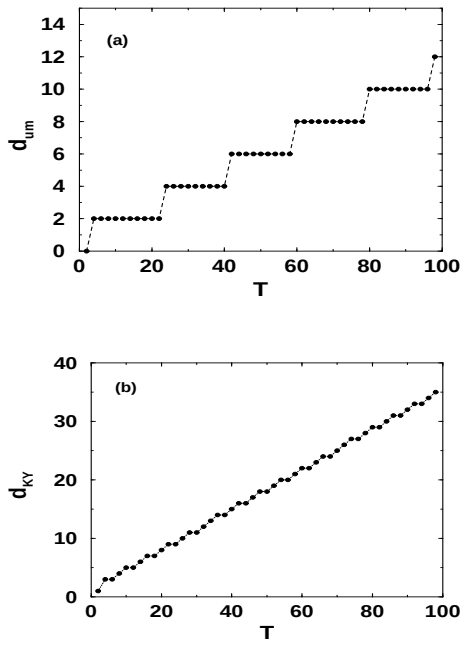

Figure 2.4: Dimensions related to periodic orbits of the Hénon map with $a = 1.0$ and $b = 0.3$.

Kaplan-Yorke dimension d_{KY} (see e.g. [1] for the statement of the Kaplan-York conjecture). of this orbit is depicted. We have obtained the same result for the dimension of the unstable manifold (d_{um}) from the winding number of $g(z) = z^{-(T+1)} - 4\overline{x}_1\overline{x}_2 z^{-T} + 2b(\overline{x}_1 + \overline{x}_2)z^{-T/2} - b^2$ along unit circle, i.e. along the path $z = e^{(i\phi)}$ with $0 \leqslant \phi \leqslant 2\pi$.

One can investigate which kind of bifurcations are associated with the steps of d_{um} in figure 2.4, using the method pointed out in section 2.2.3. We investigate the bifurcations for $1 \leqslant T \leqslant 5$ and depict the results in figure 2.5. As the delay increases and also the dimensionality of the phase space, new eigenvalues become finite growing from $-\infty$ (note this in the figure near $\tau = 1$ and $\tau = 2$). The orbit existent for odd delay values is always unstable and does not suffer bifurcation in the interval considered in the figure 2.5. On the other hand the period two orbit, is stable for $T = 2$ but unstable for $T = 4$. Let us have a closer look at the kind of bifurcation suffered by the "even" orbit, which makes it unstable at $T = 4$. A pair of eigenvalues crosses the unitary circle at the point $\tau \approx 3.833...$, the period two orbit

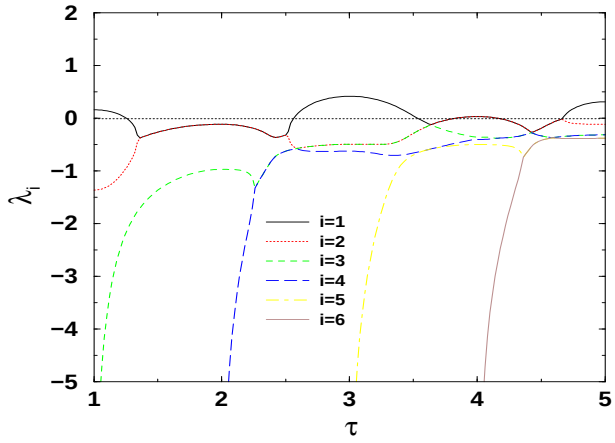

Figure 2.5: Lyapunov exponents of the period two orbits of Hénon map with $a = 1.0$ and $b = 0.3$. As the parameter τ is varied the orbit changes smoothly from that existent at even delay value to that corresponding to odd delay value.

becomes unstable and two stable invariant circles appear around it, i.e. a Neimarck-Sacker bifurcation occurs [4] - the equivalent for maps to the Hopf bifurcation (see figures 2.6 and 2.7 for details).

It is also interesting to investigate how the dimension increases when the delay has large value, i.e. which kind of bifurcation is associated with the increasing of dimensionality at $T = 24$ in figure 2.4. This is shown in figure 2.8 where it can be observed that the dimensionality of the unstable manifold increases because a pair of complex eigenvalues crosses the unit circle i.e., the bifurcation that takes place is of the same kind of that at low delay (see figure 2.5). From figure 2.4 (a) one sees that for this orbit this mechanism repeats for any delay value since the dimension of the unstable manifold increases always by two (at least up to the delay value we have observed numerically). Perhaps it is possible to find the normal form of this bifurcation (at all delay values it takes place), applying the central manifold theorem, but we have not done this procedure.

Higher periods - general orbits of Hénon map

In this subsection I focus on unstable periodic orbits of the Hénon map with parameter values corresponding to high dimensional chaotic motion. The

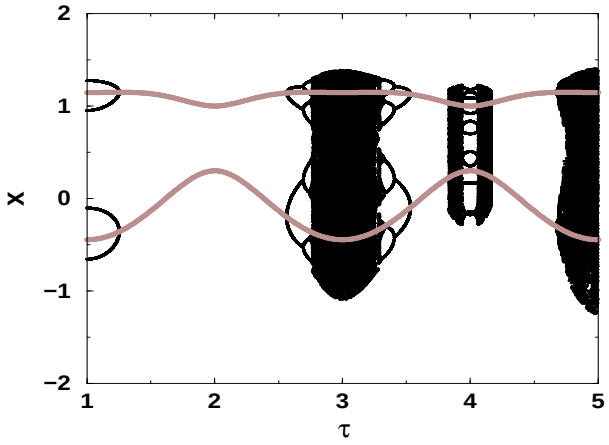

Figure 2.6: Period two orbits (white lines) and solutions (black lines) of Hénon map (2.16) modified according to Eq. (2.14), with $a = 1.0$, $b = 0.3$ Hénon map.

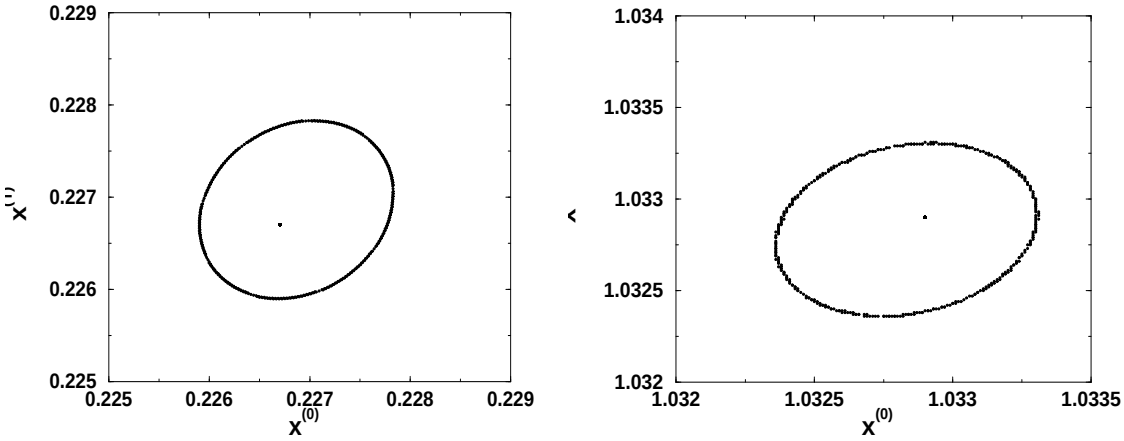

Figure 2.7: Period two orbit and invariant circle slightly beyond the Naimark-Sacker bifurcation point. Hénon map (2.16) modified according to Eq. (2.14), with $a = 1.0$, $b = 0.3$, $\tau \approx 3.833....$

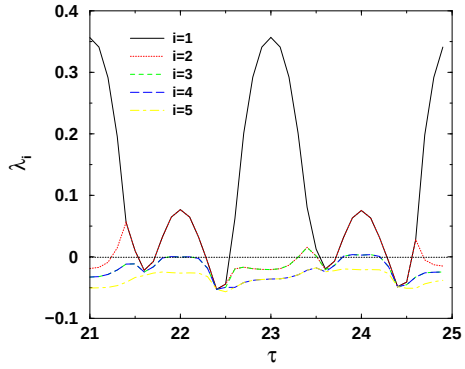

Figure 2.8: Eigenvalues of the period two orbit at delay around 22, where a second complex pair of eigenvalues crosses the unit circle: a bifurcation takes place. Hénon with $a = 1.0$ and $b = 0.3$.

first step is to recover all these cycles and the second to study their stability.

We have used the method proposed in [28] to compute the periodic orbits of the map (2.16), which was shown to be valid for the normal Hénon map for low values of the parameter b in [29]. The method is originally proposed for the two dimensional map, but was easily extended to be applied in this system. Although we have no proof that a binary partition[1] exists for the high dimensional case - which is one of the requirements for this method to work- we have evidence that most of the orbits can be recovered by the modified method.

After obtaining all the orbits and counting the number of periodic points $N(p, T)$ of each period at different delays we observe a pattern: at $p = T+1$ there is a global maximum in $N(p)$ which is followed by local maxima at $p = n(T + 1)$ (results for $T = 6, 15$ are shown in figure 2.9).

In fact, $N(p = T + 1, T)$ equals 2^p as can be evaluated from Eqs.(2.2) and (2.3) with F of Eq.(2.16), which with this special period reduces to

$$(1 - b)\overline{x}_{i+1} = a - \overline{x}_i^2 \quad . \tag{2.19}$$

After linear rescaling, Eq.(2.19) can be cast into the form of a single logistic map with parameter $a/(1 - b)^2$. As long as $a/(1 - b)^2 > 2$ this map has a full set of periodic points giving rise to the just mentioned phenomenon. At $p = n(T + 1)$ the number of periodic points is much smaller than $2^{n(T+1)}$ and we could not find a simple general rule for them.

[1] See section 4.2 for an explanation about partitions.

p	$Np(p)$	N_2
1	2	0
2	1	1
11	186	0
15	6	0
22	128	6

Table 2.1: Total number of prime orbits of period p ($Np(p)$) and number of orbits with two–dimensional unstable manifold (N_2) for the Hénon map with $a = 1.0, b = 0.3$ and $T = 10$. (Prime orbits are those which do not consist on repetitions of cycles of shorter period).

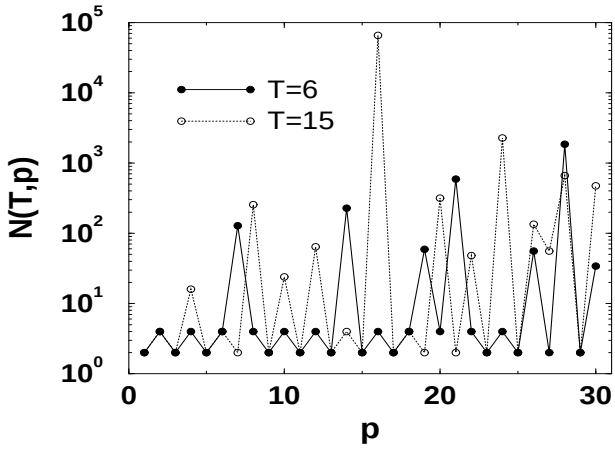

Figure 2.9: Number of p-periodic points for $T = 6$ (filled circles) and $T = 15$ (empty circles) of (2.16) with $a = 1.0, b = 0.3$.

Let us now have a closer look on the stability properties of the periodic orbits of the map (2.16). The main result is that we can divide the orbits in two categories according to the behaviour of the dimension of their unstable manifolds as a function of the delay: those for which d_{um} grows as the delay increases and those which have a $d_{um} = 1$ (i.e. only the anomalous exponent is positive) regardless of the delay value. In table 2.1 we show the periodic orbits detected by the Biham-Wenzel method up to period $p = 29$ for $T = 10$. We have observed that in this case, the orbits whose unstable manifolds have dimension equal to one are the vast majority of the computed orbits. For many of these orbits the dimension of the unstable manifold does not change if the delay is increased, the corresponding positive Lyapunov exponent stays isolated, and the remaining part of their spectrum is negative.

There exist also orbits for which the dimension of the unstable manifold increases with the delay. These orbits show up at $a = 1.0$, $b = 0.3$ and $T = 10$ with a two–dimensional unstable manifold. Although their number is very small compared to the orbits with one dimensional unstable manifold, the second kind of orbits constitute in general the less unstable. In particular we find an increasing unstable dimension as the delay increases. For instance, figure 2.4 displays this increase for the period 2 orbit of table 2.1 which exists for all even values of the delay (and was already discussed in the former section).

2.3 Periodic orbits of DDE's

In this section we describe some properties of periodic orbits of delayed difference equations of type Eq. (1.3) and its stability. Before we focus on periodic orbits, we present very briefly some properties of the stability of fixed points of Eq. (1.3), as they share many properties and the analysis of fixed point is more intuitive.

2.3.1 The stability of fixed points

The fixed points x^* of a scalar differential-difference equation of the form of Eq. (1.3) are simply the solutions of $F(x^*, x^*) = 0$ and therefore independent from the delay value τ. In this sense the problem of finding such fixed points is not different from the case of ODE's and this can be generalised to the case when x is a vector $\in \mathbb{R}^N$. One can then proceed in the analysis like in the case of an ODE and ask about the stability of such fixed points against some infinitesimal perturbation $\delta x(t) = x(t) - x^*$. Expanding Eq. (**??**)

around the fixed point and truncating in first order (this is allowed since one wants to consider only evolution of microscopic perturbations), one gets the equation for the evolution of $\delta x(t)$:

$$\dot{\delta}x(t) = C_0\delta x(t) + C_1\delta x(t-\tau) \tag{2.20}$$

where

$$\begin{aligned} C_0 &= \frac{\partial f(x_t, x_\tau)}{\partial x_t}|_{x_t=x_\tau=x^*} \\ C_1 &= \frac{\partial f(x_t, x_\tau)}{\partial x_\tau}|_{x_t=x_\tau=x^*}. \end{aligned} \tag{2.21}$$

As solutions of the linear equation (2.20) the Ansatz $\delta x(t) = e^{(\lambda t)}\delta x(0)$ can be used which leads to the characteristic equation for λ:

$$\lambda = C_0 + C_1 e^{-\lambda\tau}. \tag{2.22}$$

Such equation has an infinite number of complex solutions [2]. The stability of the linear equation (2.20) and also of other differential-difference equation with more than one delay and with a exponential distribution of delays was treated extensively in [16, 8] and also in [14] and [3]. Here, we do not enter in details but only mention some results that will assure some properties of the stability as the delay increases [16, 14] : the solutions with positive real part are isolated and their number is finite, as the delay increases it is proven that the number of such positive solutions may increase or not change in number but never decrease.

In the case of more than one delay the possible behaviours don't change much [8] and also in the case of $x \in \mathbb{R}^N$ with $N > 1$. The situation is different in equations with kernel [14].

Periodic orbits

The problem of finding the orbits and studying their stability is more subtle in the time continuous case than in the case of maps [3]. Despite of that

[2] When the delay is small, one could propose to expand $e^{\lambda\tau}$ in its polynomial series in τ and truncate at some finite degree. This procedure was tried already and it turns out not to be a good one [8] in general

[3] Although we should stress that the general problem of finding periodic orbits of non-linear mappings is not a trivial one and only methods that rely on numerics can tackle it as in e.g. [28].

difficulties there are many results in the literature treating orbits of Eq.(1.3) in the special form:

$$\dot{x}(t) = -\gamma x(t) + g(x(t-\tau)) \tag{2.23}$$

with $g(x)$ piecewise constant. This paradigm has been extensively investigated in [30] and later works of the same authors.

2.3.2 Periodic orbits at different delays

Remembering that our objective is studying the behaviour of periodic orbits as delay changes, we suppose that periodic orbits of Eq. (1.3) exist, which seems to be the case for many systems studied in the literature and derive their properties at different delays as it was done for the maps.

A bounded periodic orbit $\gamma(t)$ of period θ can be decomposed in Fourier series, i.e. we can write:

$$\gamma(t) = \sum_k A_k e^{ik\omega t} \tag{2.24}$$

with $\omega = 2\pi/\theta$ and $A_k \in \mathbb{C}$. The coefficients A_k must be such that

$$\dot{\gamma}(t) = f(\gamma(t), \gamma(t-\tau)), \tag{2.25}$$

and therefore we can conclude that the orbit is invariant under the transformation

$$\tau \to \tau + n\theta, n \in \mathbb{Z}. \tag{2.26}$$

Hence, we expect to find the same orbit (with the same period and the same coefficients A_k) at different delays as long as the delays obey relation (2.26).

Now it remains to investigate how the stability of the orbits may change as the delay increases. Following the usual procedure developed for ODE's we write the equation of the perturbation $\delta x(t) = x(t) - \gamma(t)$ around the orbit. One can use the Floquet theorem and propose the usual Ansatz for the perturbation: A periodic function times exponential dependence in time $\delta(t) = q(t)e^{\lambda t}$. The evolution equation reads:

$$\dot{\delta x}(t) = [\dot{q}(t) + \lambda q(t)]e^{\lambda t} = [C_0(t)q(t) + C_1(t)e^{-\lambda\tau}q(t-\tau)]e^{\lambda t} \tag{2.27}$$

where

$$\begin{aligned} C_0(t) &= \frac{\partial f(x_t, x_\tau)}{\partial x_t}|_{x_t, x_\tau \in \gamma(t)} \\ C_1(t) &= \frac{\partial f(x_t, x_\tau)}{\partial x_\tau}|_{x_t, x_\tau \in \gamma(t)} \end{aligned} \tag{2.28}$$

The most general formulation of the Floquet eigenmodes in delayed systems is presented in [31]. Here we don't discuss this issue but only point out that since the orbit is the same, so does the function $q(t)$ and consequently the coefficients $C_0(t)$, $C_1(t)$ i.e. the delay enters only in the exponential resembling the case of the fixed points. The equation is however more complicated and we could not find out if an asymptotic form of the spectrum of eigenvectors also exists in this case as in that of maps.

2.3.3 Analysis of orbits with period $\theta = \frac{p}{q}\tau$

In the special case when $\theta = \frac{p}{q}\tau$ the Eq.(2.25) reduces to a set of ODE's:

$$\begin{aligned} \dot{x}^{(i)}(t) = f(x^{(i)}(t), x^{(i+1)}(t)), \quad 0 \leqslant i < p-1 \\ \dot{x}^{(p-1)}(t) = f(x^{(p-1)}(t), x^{(0)}(t)) \end{aligned} \tag{2.29}$$

with $x^{(i)}(t) = x(t - i\tau)$. As a consequence, one can apply methods developed for ODE's to detect the periodic orbits with these special periods. To be precise, however, one has to prove that all periodic orbits of the system of Eqs.(2.29) correspond of orbits of Eq.(1.3). Although we have not done this analytically nor investigated numerically the validity of this scheme, we proceed in the formulation and write the equation of stability (the differential equation in the tangent space) using these ideas.

As pointed out in [31] the stability equation for this case can be expressed as a set of ODE's constructing perturbation vector $\delta\mathbf{x}(t) \in \mathbb{R}^p$ with components $\delta x^{(i)}(t) = \delta x(t - i\tau)$ and using the Floquet Ansatz, we have:

$$\begin{aligned} \delta x^{(i)}(t) = e^{-\lambda i\tau} e^{\lambda t} q^{(i)}(t) \\ q^{(i)}(t) = q(t - i\tau) \end{aligned} \tag{2.30}$$

and the evolution equation of each component:

$$\dot{\delta x}^{(i)}(t) = C_0^{(i)}(t)\delta x^{(i)}(t) + C_1^{(i)}(t)\delta x^{(i+1)}(t) \tag{2.31}$$

which can be written as

$$\dot{\delta x}^{(i)}(t) = [C_0^{(i)}(t)q^{(i)}(t)e^{-\lambda i\tau} + C_1^{(i)}(t)e^{-\lambda(i+1)\tau}q^{(i+1)}(t)]e^{\lambda t} \tag{2.32}$$

with

$$\begin{aligned} C_0^{(i)}(t) = \frac{\partial f(x_t, x_\tau)}{\partial x_t}|_{x_t = x^{(i)}(t), x_\tau = x^{(i+1)}(t)} \\ C_1^{(i)}(t) = \frac{\partial f(x_t, x_\tau)}{\partial x_\tau}|_{x_t = x^{(i)}(t), x_\tau = x^{(i+1)}(t)} \end{aligned} \tag{2.33}$$

Making the transformation $\delta x^{(i)}(t) \rightarrow \delta x^{(i)}(t)e^{\lambda i \tau}$, the evolution equation for the vector $\delta \mathbf{x}$, reads

$$\dot{\delta \mathbf{x}}(t) = \mathbf{J}(t,\lambda)\delta \mathbf{x}(t) \tag{2.34}$$

where the matrix $\mathbf{J}(t,\lambda)$ has the form:

$$\mathbf{J}(t,\lambda) = \begin{pmatrix} C_0^{(0)}(t) & C_1^{(0)}(t)e^{-\lambda\tau} & 0 & ... & 0 \\ 0 & C_0^{(1)}(t) & C_1^{(1)}(t)e^{-\lambda\tau} & ... & 0 \\ & \ddots & & & \\ C_1^{(p-1)}(t)e^{-\lambda\tau} & 0 & ... & 0 & C_0^{(p-1)}(t) \end{pmatrix}$$

We may also write:

$$\delta \mathbf{x}(t) = \mathbf{U}(t,\lambda)\delta \mathbf{x}(0) \tag{2.35}$$

where the matrix obeys the linear evolution equation

$$\dot{\mathbf{U}}(t,\lambda) = \mathbf{J}(t,\lambda)\mathbf{U}(t,\lambda) \tag{2.36}$$

and therefore $\mathbf{U}(t,\lambda) = T[e^{\int_0^t \mathbf{J}(s,\lambda)ds}]$ with T indicating the time ordering product.

Using the initial Ansatz, we may write $\delta \mathbf{x}(\theta) = e^{\lambda\theta}\delta \mathbf{x}(\theta)$ and combining with Eq.(2.35) we arrive at the characteristic equation

$$det[\mathbf{U}(\theta, z^{-\frac{\tau}{\theta}}) - z\mathbb{I}] = 0 \tag{2.37}$$

where we have made $z = e^{\lambda\theta}$. Making $z = \mu^{-p}$ and remembering that $\tau/\theta = p/q$ such equation can be written as

$$det[\mu^p \mathbf{U}(\theta, \mu^q) - \mathbb{I}] = g(\mu) = 0 \tag{2.38}$$

and one can obtain the dimension of the unstable manifold of the orbtis from the winding number of $g(\mu)$ as described in [26] (in the context of chaos control).

Knowing that every orbit is conserved under the transformation (2.26), one might wonder what happens to its stability as the delay increases. In the case of special orbits treated here, Eq.(2.26) corresponds to a change in the value of q, but not on p. The structure of Eq. (2.38) is maintained as the delay increases by multiples of the orbit, only the value of q is transformed like $q \rightarrow q + n$.

2.3.4 Summary

To sumarize we have seen that it is rather difficult to get detailed information about all periodic orbits of Eqs.(1.3) and (1.4). Nonetheless, some important properties under change of delay value have been discussed in this chapter. The two most relevant restults are the existence of the same orbit at different delay values, and for the case of maps the existence of an asymptotic spectrum of Lyapunov exponents due to an asymptotic form of the characteristic equation for delayed maps.

Chapter 3

All trajectories: Invariant densities

3.1 Scalar densities at large delay

In this chapter we will leave the individual periodic solutions and focus on the behavior of chaotic attractors of delayed systems, in the regime of the feedback time τ where the asymptotics of the Kaplan Yorke dimension and of the information entropy can be observed. In fact, these scaling properties are a consequence of the asymptotic behaviour of the Lyapunov spectrum in the limit $\tau \to \infty$. Being ergodic averages, Lyapunov exponents reflect two important aspects of the dynamics: the linear (in-)stability and the statistical properties. The latter depend directly on the invariant density of a system. In order to gain some insight in this "universal" regime of high dimensional chaos of delayed systems, the understanding of the properties of invariant densities of delayed systems in the limit of large delay is an essential and nontrivial starting point.

The investigation carried out here, is motivated by the following numerically observed phenomenon: By ergodicity, a single solution $x(t)$ creates a natural invariant density called $\rho_\tau(x)$, if transients are discarded. This marginal density is one particular projection of the full phase space density as it is observed to possess a well defined asymptotic form $\rho_\infty(x)$ in the limit of large delay (see figure 3.1 for an example, where an asymptotic form exists in a range of delay values). The main issue of this chapter is to study under which conditions and how this density $\rho_\tau(x)$ converges to an asymptotic form $\rho_\infty(x)$ in the limit of large τ , and what are the underlying

mechanisms for this convergence.

One could argue that this behaviour is not surprising: As the dimensions of the attractors grow and more degrees of freedom become relevant one could expect that the projection of the measures onto any space with much smaller dimension than the attractor itself will be smooth and not depend on the delay. This would be a consequence of the central limit theorem. But this is far from being the correct explanation: the degrees of freedom are correlated and the one dimensional distribution is typically not Gaussian (as the argument would predict) but strongly dependent on the system. The idea of using the central limit theorem was, however, successfully explored in [22], when treating equations of the type (I):

$$\dot{x} = -x(t) + kg(x(t-\tau)). \tag{3.1}$$

Therein the authors are able to construct a version of the central limit theorem to derive the invariant density of uncorrelated points. Although this treatment is very illustrative it is not general, and its success will depend strongly on the value of k and on the properties of $g(x)$, i.e. only for large k and oscillating $g(x)$ the loss of memory is achieved which allows treating the equation above in the same way as a Langevin equation, where the role of noisy perturbation is played by the delayed feedback. In this limit, x has Gaussian invariant density.

The concrete treatment of problems related to the invariant density of (1.3) will at some point require discretisation of time as done in [32, 22]. Therefore one will be treating the problem of a map that in some limit will describe very well the behaviour of the continuous time system. Since we are interested in fundamental issues and not in the behaviour of a special system, we decided to treat directly scalar delayed maps of the form of Eq.(1.4) for which we have observed that the probability density $\rho_T(x)$ of x_n induced by a stationary invariant density in the finite $(T+1)$ -dimensional phase space will have an asymptotic form for large delay - $\rho_\infty(x)$. Therefore, in this sense delayed maps and DDE's show similar behaviours.

Before entering in details on the invariant density of delayed maps, we describe briefly the conventional formalism adopted to investigate invariant densities of maps. We introduce the Frobenius-Perron operator and other concepts which will be important in our analysis in a non-rigorous fashion, following the descriptions in [33] and [34]. More formal considerations can be found in [35].

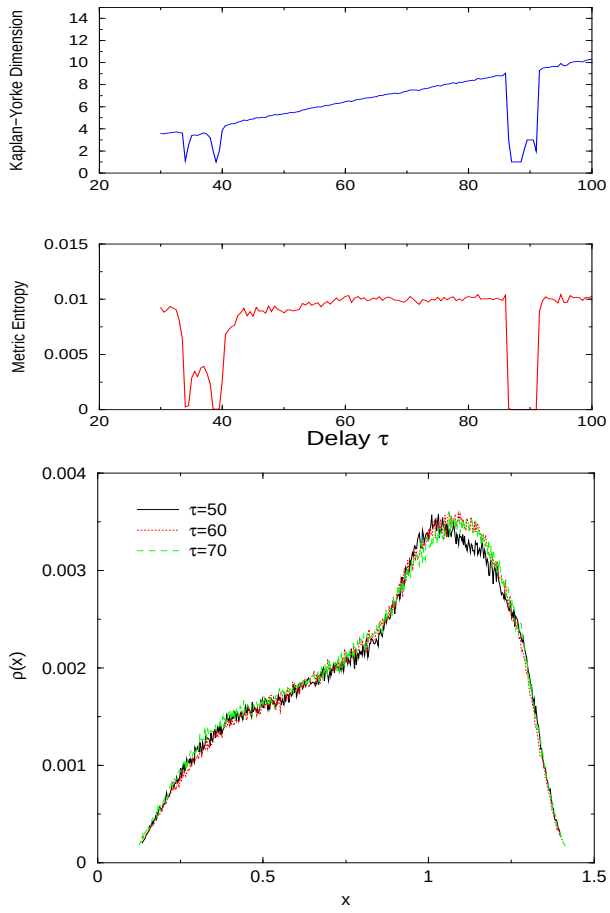

Figure 3.1: Some properties of the Mackey-Glass equation $\dot{x} = -bx(t) + \frac{ax(t-\tau)}{(1+x(t-\tau)^{10})}$ with $a = 0.2$ and $b = 0.1$. Upper panel: Dimension, entropy as a function of the delay τ. Lower panel: probability densities constructed from the time series of $x(n\Delta t)$ with $\Delta t = 0.001\tau$ (integration step).

3.2 Evolving densitities

Trajectories of chaotic dynamical systems diverge exponentially and an initial condition known with a limited precision gives rise to unpredictable behavior after finite time. Writing an equation for each individual possible trajectory of such a system is an unimaginable task: Due to sensitivity to initial conditions two infinitely close initial conditions will lead to completely different outcomes in the long term. Hence, more meaningful than following individual trajectories, is to investigate how densities (smooth distributions of initial conditions) evolve in time under a chaotic mapping.

3.2.1 Frobenius-Perron operator

In order to formulate the evolution of densities in a proper way we must describe a measure $d\mu(\mathbf{x}) = \rho(\mathbf{x})d\mathbf{x}$, whose mass over a subset X_i of the whole phase space X:

$$\Delta\mu_i = \int_{X_i} d\mu(x) = \int_{X_i} \rho(\mathbf{x})d\mathbf{x} \tag{3.2}$$

where $\rho(\mathbf{x})$ is the density of representative points in the phase space. The density $\rho(\mathbf{x})$ must be such that integrals of type (3.2) are positive and finite, and that it can be normalised:

$$\int_X \rho(\mathbf{x})d\mathbf{x} = 1. \tag{3.3}$$

Apart from these restrictions, the densities might be ill defined and be confined to a fractal support, i.e. can contain distribution-like components such as Dirac deltas. The measure, on the contrary, is a better behaved function of sets.

Given an initial density $\rho_n(\mathbf{x})$ with support on a region X_i and a map $M : \mathbf{x}_{n+1} = f(\mathbf{x}_n)$ where $\mathbf{x} \in \mathbb{R}^d$, the question is how this density evolves in time under this map. Iterating once the map, the region X_i is carried into $f(X_i)$ and due to conservation of representative points one has:

$$\int_{f(X_i)} \rho_{n+1}(\mathbf{x})d\mathbf{x} = \int_{X_i} \rho_n(\mathbf{y})d\mathbf{y}. \tag{3.4}$$

Since we want to obtain the expression for $\rho_{n+1}(\mathbf{x})$ as a function of $\rho_n(\mathbf{x})$, we transform the integration variable from x to $\mathbf{y} = f^{-1}(\mathbf{x})$ in the R.H.S of

Eq.(3.4):

$$\int_{X_i} \rho_{n+1}(\mathbf{y})|det\mathbf{J}(\mathbf{y})|d\mathbf{y} = \int_{X_i} \rho_n(\mathbf{y})d\mathbf{y} \tag{3.5}$$

where $\mathbf{J}(\mathbf{y}) = \frac{\partial f(\mathbf{y})}{\partial \mathbf{y}}$ is the Jacobian matrix of the map. The density $\rho_{n+1}(\mathbf{x})$ can be written as:

$$\rho_{n+1}(\mathbf{x}) = L_f\rho_n(\mathbf{x}) = \sum_{\mathbf{y}_i=f^{-1}(\mathbf{x})} \frac{\rho_n(\mathbf{y}_i)}{|det\mathbf{J}(\mathbf{y}_i)|} \tag{3.6}$$

or as:

$$\rho_{n+1}(\mathbf{x}) = L_f\rho_n(\mathbf{x}) = \int_X \delta(\mathbf{x} - f(\mathbf{y}))\rho_n(\mathbf{y})d\mathbf{y}. \tag{3.7}$$

and L_f is the so called Perron-Frobenius operator which is a linear operator that acts on the space of integrable functions. By working with densities instead of trajectories one exchanges a finite dimensional nonlinear mapping by a linear operator acting on an infinite dimensional function space.

3.2.2 Invariant densities, ergodicity and mixing

Particularly important in the theory of dynamical systems are the so called invariant densities: They are simply fixed points of the operator L_f, i.e. an invariant density $\rho(\mathbf{x})$ fulfils the condition:

$$\rho(\mathbf{x}) = L_f\rho(\mathbf{x}) = \int_X \delta(\mathbf{x} - f(\mathbf{y}))\rho(\mathbf{y})d\mathbf{y}. \tag{3.8}$$

Finding these fixed points rigorously is not a trivial task, there are many results for one dimensional maps [34], but usually the invariant densities do exist and might be more than one for a given map [1].

Having an invariant density, it is possible to introduce the expectation value, or ensemble average of an arbitrary test function $g(\mathbf{x})$ with respect to it:

$$< g >= \int_X g(\mathbf{x})\rho(\mathbf{x})d\mathbf{x}. \tag{3.9}$$

Due to the invariance property, the same result for $< g >$ is obtained if one replaces $\mathbf{x}$ by $f(\mathbf{x})$ in Eq. (3.25), i.e. expectation values of the variables in the invariant ensemble are invariant under the action of f.

[1] E.g. each periodic orbit of f is associated with an invariant density : $\rho(\mathbf{x}) = \frac{1}{p}\sum_i^p \delta(\mathbf{x} - \overline{\mathbf{x}}_i)$.

In the same way, one can define the time average of g with respect to a trajectory:

$$\overline{g} = \lim_{N\to\infty} \frac{1}{N} \sum_{n=0}^{N} g(\mathbf{x}_n) \tag{3.10}$$

which is different from $< g >$ and depends on the initial condition x_0.

Knowing these two averages it is possible to define ergodicity of a map (in a non rigorous way): A map together with an invariant density is said to be ergodic if for any integrable function g the time average is equal to the phase space average with respect to $\rho(\mathbf{x})$, i.e. for any $\mathbf{x}_0$, up to a set of measure zero one has $\overline{g} =< g >$. Ergodicity implies that time averages do not depend on the initial condition $\mathbf{x}_0$ up to some exceptional values. Alternatively one might say that a map is ergodic on one particular support, since similarly as there might coexist several invariant measures, there might coexist also several ergodic components of the phase space.

An ergodic map might possess many invariant densities, but only one is meaningful from the physical point of view: The so called natural invariant density which is obtained almost surely if a random initial condition is iterated, i.e. it can be described by:

$$\rho(\mathbf{x}) = \lim_{N\to\infty} \frac{1}{N} \sum_{n=0}^{N} \delta(\mathbf{x} - \mathbf{x}_n). \tag{3.11}$$

An even stronger property than ergodicity is the mixing property. A map is called mixing if an arbitrary smooth initial probability density $\rho_0(\mathbf{x})$ converges to the natural invariant density $\rho(\mathbf{x})$ under successive interactions of the map:

$$\lim_{n\to\infty} \rho_n(\mathbf{x}) = \rho(\mathbf{x}) \qquad \forall \qquad smooth \qquad \rho_0(\mathbf{x}). \tag{3.12}$$

This property can be described more precisely considering two subsets of the phase space, say A and B, saying that a map mixing if:

$$\lim_{n\to\infty} \mu(f^n(A) \wedge B) = \mu(A)\mu(B). \tag{3.13}$$

Through this formulation it becomes clear that the generalised correlation function asymptotically decays to zero, i.e. mixing means asymptotic statistical independence in its most strict sense. Although mixing implies ergodicity the reverse is not true.

Constructing measures from trajectories

An ergodic map has an interesting property: Its natural invariant measure can be recovered just iterating a single initial condition and producing a histogram, i.e. counting the relative frequency of iterates in a certain subset X_i of the phase space. This can be easily seen if we choose for $g(\mathbf{x}) = \Theta_{X_i}(\mathbf{x})$ in Eq. (3.10) a function that is 1 if $\mathbf{x} \in X_i$ and zero otherwise. Then from Eqs.(3.10) and (3.25) one gets:

$$\lim_{N\to\infty} \frac{1}{N} \sum_{n=0}^{N} \Theta_{X_i}(\mathbf{x}) = \int_{X_i} \Theta_{X_i}(\mathbf{x})\rho(\mathbf{x})d\mathbf{x} = \mu(X_i). \tag{3.14}$$

Exactly this method will be used in the next section to estimate the invariant measure of the delayed maps.

3.3 Formulating the problem

3.3.1 The issue in detail: numerics for a simple map

In many different delayed systems we have observed an asymptotic behaviour of the projections of the invariant measure at large delays. As an example consider the map:

$$x_{n+1} = (1-\epsilon)f(x_n) + \epsilon f(x_{n-T}), \tag{3.15}$$

where $f(x) = 2x - \mathrm{sgn}(x), \quad x \in [-1, 1]$. In figure 3.2 we present the numerical results on how the density of the variable x converges to an asymptotic form as the delay increases. The densities were obtained by dividing the interval $[-1, 1]$ in cells I_x of equal size centred at a point x. The density $\mu(x)$ is computed from a normalised histogram (relative visiting frequency of cell I_x). We have defined a quantity to characterise the difference between these invariant densities at low and large delay: $\sum_{I_x} |\mu_T(x) - \mu_\infty(x)|$. Its dependence on the delay value is depicted in figure 3.3. This quantity converges to zero (at least within the numerical error) as $T \to \infty$. The convergence behavior depends on details of the system (here the parameter ϵ). In the special case of $\epsilon = 0.5$, the measure has the form $\mu(x) \propto 2x - \mathrm{sgn}(x)$ and is independent of T. As the densities are non Gaussian, we do not expect that the simple central limit theorem will supply justification for the convergence. In fact, as it will be seen later, the variables are not completely

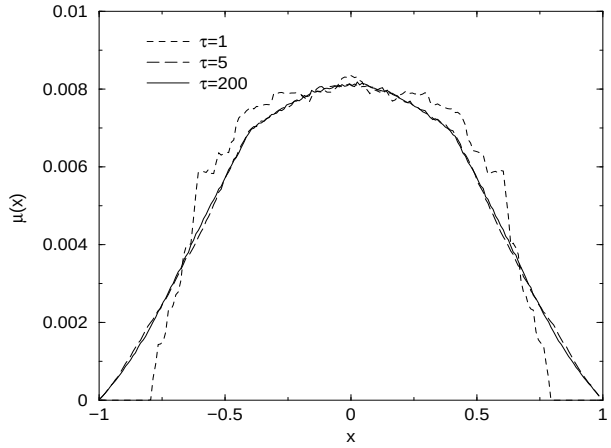

Figure 3.2: The invariant density of equation (3.15) for a definite T and $\epsilon = 0.3$. $\mu(x)$ is estimated by a normalised histogram. The interval $[-1, 1]$ is divided into 200 cells and we have used a time series of 10^6 points.

uncorrelated. Moreover, the arguments applied in [22] to study the density of Eq.(3.1), cannot be applied here even in the limits $\epsilon \to 0$ and $\epsilon \to 1$.

In order to observe if there is some decoupling of the degrees of freedom we define a quantity

$$\Delta(j) =< |\mu(x_n, x_{n-j}) - \mu(x_n)\mu(x_{n-j})| > \tag{3.16}$$

where the two dimensional density $\mu(x_n, x_{n-j})$ is estimated dividing the plane in square cells centred at $\{x_n, x_{n-j}\}$ and constructing the corresponding histogram from a time series. The average in (3.16) is computed over the cells. This quantity has similar meaning as the mutual information: It describes the distance between two densities. The nearer the quantity is to zero, the more uncorrelated are x_n and x_{n-j}. This is a stronger test for uncorrelation than the linear correlation would provide. In figure 3.4 the dependence of Δ on j is depicted for different values of ϵ. Due to statistical errors existent on the measure at every box, the value $\Delta = 0$ is never achieved. We could instead identify a finite minimum value for Δ at every simulation (the plateau in figure 3.4). We consider that the variables are uncorrelated when Δ assumes this minimum value, what is justified through the following simple consideration: Taking two different initial conditions, x and y, we compute $< \mu(x_n, y_n) - \mu(x_n)\mu(y_n) > \approx \Delta$, since by construction

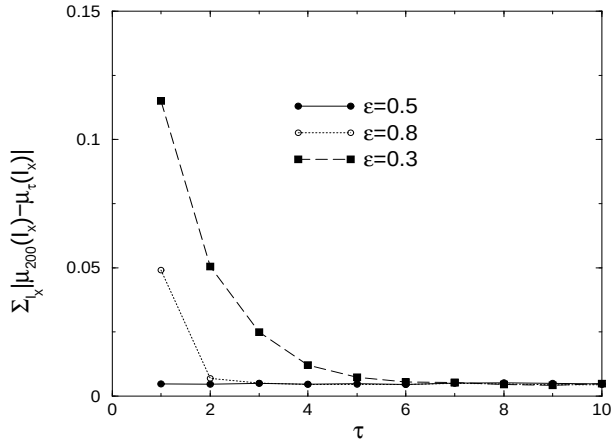

Figure 3.3: Difference between the measures μ_T and μ_{200} (representing μ_∞) as a function of T. The measure is estimated in the same way as in figure 3.2. The sum is performed over the cells as described in the text.

x and y are independent we hence check the value of the systematic finite sample error.

By comparing the figures 3.3 and 3.4 one might wonder if the convergence of the one-dimensional projection of the measure is a consequence of the loss of correlations at short time scales. This seems not to be true as it will be seen later on.

Another way to look at the map of Eq. (3.15) is considering it acting on a $T+1$ dimensional space, defining the components of the vector $\mathbf{x} \in \mathbb{R}^{T+1}$ by $x^{(j)} = x_{n-j}$. One might then ask if other low dimensional projections of the invariant density, e.g. two dimensional projections $\rho(x^{(i)}, x^{(j)})$, will also possess an asymptotic form in the limit of large delay. Investigating numerically two dimensional densities of the map Eq.(3.15), we could find similar results as those observed for one dimensional densities. This gives us some reasons to believe that other low dimensional projections should exhibit the same behavior.

3.3.2 Transporting densities of delayed maps

In order to investigate formally the invariant measures, we have to construct the Frobenius-Perron equation and try to understand the observed numerical facts from it. There are two different approaches to construct these equations

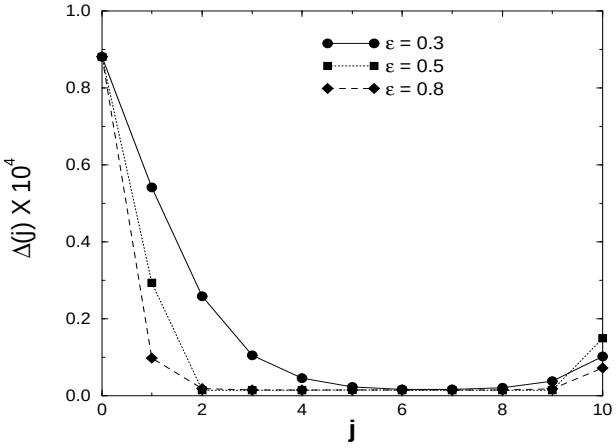

Figure 3.4: $\Delta(x_n, x_{n-j})$ for the map (3.15) with delay $T = 10$. The measures are estimated from the relative frequencies at cells on a plane and the average is performed over the cells. A time series of 10^7 point is used.

in the case of delayed maps.

One way (proposed in [27]) is to consider the T–time distributions

$$\begin{aligned} \rho^{(1)}(x) &= \langle \delta(x - x_n) \rangle \\ \rho^{(2)}(x,y) &= \langle \delta(x - x_n)\delta(y - x_{n-T}) \rangle \\ \rho^{(3)}(x,y,z) &= \langle \delta(x - x_n)\delta(y - x_{n-T})\delta(z - x_{n-2T}) \rangle \\ &\vdots \end{aligned} \tag{3.17}$$

where $\langle \ldots \rangle$ denotes the average over x_n with respect to the natural invariant density (i.e. a long time average), then invariance yields the system of equations for a map like Eq. (3.1):

$$\begin{aligned} \rho^{(1)}(x) &= \int dx' \int dy'\, \delta(x - f(x',y'))\rho^{(2)}(x',y') \\ \rho^{(2)}(x,y) &= \int dx' \int dy' \int dz'\, \delta(x - f(x',y')) \\ &\quad \times \delta(y - f(y',z'))\rho^{(3)}(x',y',z') \\ &\vdots \end{aligned} \tag{3.18}$$

which corresponds to an open hierarchy of equations, that cannot be solved unless some simple Ansatz is assumed, e.g. assuming that $\rho^{(2)}(x,y) =$

$\rho^{(1)}(x)\rho^{(1)}(y)$. An interesting feature of the system (3.18) is that it does not depend explicitly on the delay value, while one expects that the invariant density does. The dependence comes implicitly in the fact that correlations e.g. between x and y would depend on the delay value.

Another approach consists in considering the vectorial form of Eq. (3.1), whose Frobenius-Perron equation reads

$$\rho(x^{(0)},\ldots,x^{(T)}) = \int dz\delta(x^{(0)} - f(x^{(1)},z))\rho(x^{(1)},\ldots,x^{(T)},z) \qquad (3.19)$$
$$= \sum_{z_i/x^{(0)}=f(x^{(1)},z_i)} \frac{\rho(x^{(1)},\ldots,x^{(T)},z_i)}{\partial f(x^{(1)},z_i)/\partial z}.$$

Its solution determines the two time density

$$\rho^{(2)}(x,y) = \int dx^{(1)} \ldots \int dx^{(T-1)}\rho(x,x^{(1)},\ldots,x^{(T-1)},y). \qquad (3.20)$$

Hence, one quantity in the system (3.18) is fixed, and by condition (3.20) the delay time enters explicitly. Therefore, an analysis which is based solely on Eqs.(3.18) does not seem to be consistent.

Before we continue with the analysis it is worth to highlight some features of Eq. (3.19). First it is possible to see that the structure of Eq.(3.19) does not change as the delay increases, e.g. the number of pre-images of a given point is conserved and this will allow us to make a statement about the entropy in chapter 4. On the other hand, the structure does not assure that the solutions will be identical: As the dimensionality of the vector changes, the function $\rho(\mathbf{x})$ must assume different forms.

Returning now to our analysis, consider equations (3.18): We see that $\rho^{(1)}$ is fully determined if $\rho^{(2)}$ is known. If $\rho^{(2)}$ has a definite asymptotic form in the limit $T \to \infty$ so does $\rho^{(1)}$, according to (3.18). Determining $\rho^{(2)}$ seems to be only possible by solving the Frobenius-Perron equation (3.19), which is a difficult task particularly at the limit of large T. In order to investigate further this problem we have chosen a special case of a delayed system where the invariant measure can be investigated analytically.

3.4 Perturbation theory for shifts on a torus

Since a general approach seems to be too ambitious in this case, we have chosen a map on a torus, i.e. we consider its variable φ as an angle, in order

to perform some analytical investigations. Such maps are known to have nice properties from the analytical point of view, e.g. they are hyperbolic if local expansion rates are positive and allow for perturbation expansions (cf. e.g. [36] for an application in the context of coupled map lattices). Since we will base part of our analysis on such expansions we consider the following map defined on the circle:

$$\varphi_{n+1} = 2\varphi_n + \varepsilon g(\varphi_n) + \varepsilon g(\varphi_{n-T}) \tag{3.21}$$

where the variable φ is considered modulo 2π and ε will later on be a small parameter giving rise to a perturbation theory. We may also express this map in a vector space considering $\boldsymbol{\phi}$ as vector with components $\phi^{(0)}, \phi^{(1)}, ..., \phi^{(T)}$ where $\phi_n^{(i)} = \varphi_{n-i}$:

$$\begin{aligned} \phi_{n+1}^{(0)} &= 2\phi_n^{(0)} + \varepsilon g(\phi_n^{(0)}) + \varepsilon g(\phi_n^{(T)}) = f(\phi^{(0)}, \phi^{(T)}) \\ \phi_{n+1}^{(i)} &= \phi_n^{(i-1)} \qquad 1 \leqslant i \leqslant T \end{aligned} \tag{3.22}$$

i.e. $\boldsymbol{\phi_{n+1}}=F(\boldsymbol{\phi_n})$. We can write the Frobenius-Perron equation for this system in this $(T+1)$-dimensional space as:

$$\rho_{n+1}(\boldsymbol{\phi}) = \int d\boldsymbol{\phi'}\, \delta(\boldsymbol{\phi} - F(\boldsymbol{\phi'})\rho_n(\boldsymbol{\phi'}) \tag{3.23}$$

Switching now to the Fourier decomposition

$$\rho_n(\boldsymbol{\phi}) = \sum_{\mathbf{k}} c_n(\mathbf{k}) e^{i\mathbf{k}\cdot\boldsymbol{\phi}}, \quad c_n(\mathbf{k}) = \frac{1}{(2\pi)^{T+1}} \int d\boldsymbol{\phi} e^{-i\mathbf{k}\cdot\boldsymbol{\phi}} \rho_n(\boldsymbol{\phi}) \tag{3.24}$$

Eq. (3.23) reads:

$$c_{n+1}(\mathbf{k}) = \sum_{\mathbf{k}'} L_{\mathbf{k},\mathbf{k}'} c_n(\mathbf{k}') \tag{3.25}$$

where

$$L_{\mathbf{k},\mathbf{k}'} = \Gamma(k'^{(0)} - 2k^{(0)} - k^{(1)}, k^{(0)}) \Gamma(k'^{(T)}, k^{(0)}) \prod_{j=1}^{T-1} \delta_{k'^{(j)}, k^{(j+1)}} \tag{3.26}$$

and the abbreviation

$$\Gamma(k', k) = \frac{1}{2\pi} \int d\phi e^{ik'\phi - ik\varepsilon g(\phi)} \tag{3.27}$$

has been introduced taking the delay into account.

3.4.1 Approximation for small ε

We expand Eq. (3.27) in terms of ε:

$$\Gamma(k',k) = \delta_{k',0} - ik\varepsilon G_{k'} + \mathcal{O}(\varepsilon^2) \tag{3.28}$$

where $G_{k'}$ are the Fourier coefficients of g.

Evaluating Eq.(3.25) for $\varepsilon = 0$ we have

$$c_{n+1}(k^{(0)},k^{(1)},k^{(3)},...,k^{(T-1)},k^{(T)}) = c_n(2k^{(0)}+k^{(1)},k^{(2)},k^{(3)},...,k^{(T)},0) \tag{3.29}$$

and thus

$$c_{n+T}(k^{(0)},k^{(1)},k^{(3)},...,k^{(T-1)},k^{(T)}) = c_n(N_T(\mathbf{k}),0,...,0,0,0) \tag{3.30}$$

where the notation

$$N_\nu(\mathbf{k}) = 2^\nu k^{(0)} + 2^{\nu-1}k^{(1)} + ... + k^{(\nu)} \tag{3.31}$$

for the argument of the Fourier coefficients has been used. If we consider an analytic density at time $n = 0$, then its Fourier coefficients decay exponentially. Thus, iterating the system (3.29) we recognise that all coefficients but a few become exponentially small and we end up with the stationary solution

$$c_*^{(0)}(\mathbf{k}) = \delta_{N(\mathbf{k}),0}. \tag{3.32}$$

The form of the invariant density in the whole phase space is the following:

$$\rho(\boldsymbol{\phi})|_{\varepsilon=0} = \sum_{\mathbf{k}} \delta_{N(\mathbf{k}),0} e^{i\mathbf{k}\cdot\boldsymbol{\phi}} \tag{3.33}$$

and it consists of one dimensional strips with uniform density. The projection of this invariant density on one dimension is uniform. The picture of the strips can be seen easily in two dimensions. For instance considering the projections on the planes $(\phi^{(0)},\phi^{(j)})$ one has:

$$\rho^{(0)}(\phi^{(0)},\phi^{(j)})\Big|_{\varepsilon=0} = \delta(\phi^{(0)} - 2^{-j}\phi^{(j)}) \tag{3.34}$$

and for large j the strips practically fill the plane. These results of course follow from analysing the map without the delayed term.

We use the series expansion

$$c_n(\mathbf{k}) = c_n^{(0)}(\mathbf{k}) + \varepsilon c_n^{(1)}(\mathbf{k}) + \mathcal{O}(\varepsilon^2) \tag{3.35}$$

to determine the stationary solution for non vanishing ε. Combining Eqs. (3.25), (3.28) and (3.35) we obtain

$$\begin{aligned} c^{(1)}_{n+1}(\mathbf{k}) &= c^{(1)}_n(2k^{(0)}+k^{(1)},k^{(2)},...,k^{(T)},0) \\ &- ik^{(0)}\sum_{\mathbf{k}'}[\delta_{k'^{(T)},0}\delta_{N(\mathbf{k}'),0}G_{k'^{(0)}-k^{(1)}-2k^{(0)}} + \\ &G_{k'^{(T)}}\delta_{N(\mathbf{k}'),0}\delta_{k'^{(0)},2k^{(0)}+k^{(1)}}]\prod_{j=1}^{T-1}\delta_{k'^{(j)},k^{(j+1)}} \end{aligned} \tag{3.36}$$

Using similar arguments as before, we obtain a stationary solution for the first order coefficients that reads

$$\begin{aligned} c^{(1)}_*(\mathbf{k}) &= -i\sum_{\nu=0}^{\infty}2^\nu N_T(\mathbf{k})\sum_{\mathbf{k}'}[\delta_{k'^{(T)},0}\delta_{N_T(\mathbf{k}'),0}G_{k'^{(0)}-2k^{(0)}-k^{(1)}} + \\ &G_{k'^{(T)}}\delta_{N_T(\mathbf{k}'),0}\delta_{k'^{(0)},2k^{(0)}+k^{(1)}}]\times\prod_{j=1}^{T-1}\delta_{k'^{(j)},0} \end{aligned} \tag{3.37}$$

$$\begin{aligned} &- i\sum_{\nu=0}^{T-1}N_\nu(\mathbf{k})\sum_{\mathbf{k}'}[\delta_{k'^{(T)},0}\delta_{N(\mathbf{k}'),0}G_{k'^{(0)}-2k^{(0)}-k^{(1)}} + G_{k'^{(T)}}\delta_{N(\mathbf{k}'),0}\delta_{k'^{(0)},2k^{(0)}+k^{(1)}}] \\ &\times\prod_{j=1}^{T-\nu-1}\delta_{k'^{(j)},k^{j+\nu+1}}\prod_{j=T-\nu}^{T-1}\delta_{k'^{(j)},0} \end{aligned} \tag{3.38}$$

Now, we have an approximation for the invariant density up to first order. We are interested in the behaviour of the low dimensional projections of this invariant density and their dependence on the delay time T. Let us first consider the one variable distribution: its expression is obtained considering $k^{(1)} = k^{(2)} = ... = k^{(T)} = 0$ in Eq.(3.24). We therefore make this substitution in Eq. (3.37) to obtain the form of the corresponding Fourier coefficients:

$$c(k^{(0)}) = \delta_{k^{(0)},0} + \varepsilon c^{(1)}(k^{(0)}) + O(\varepsilon^2) \tag{3.39}$$

from which one can see that $\varepsilon = 0$ the measure coincides with a uniform measure what is expected looking at Eq. (3.21). The first order contribution in Eq. (3.39) is given by

$$c^{(1)}(k^{(0)}) = -ik^{(0)}\sum_{\nu=0}^{\infty}2^\nu G_{-2^{\nu+1}k^{(0)}} - ik^{(0)}\sum_{\nu=0}^{\infty}2^\nu G_{-2^{T+\nu+1}k^{(0)}} \tag{3.40}$$

and we can see that if g is a smooth function, this contribution will aquire an asymptotic form in the limit $T \to \infty$.

The same procedure can be applied to obtain two–dimensional projections. Considering for instance $k^{(i)} = 0$, for any $i \neq 0$ and $i \neq j$ we may obtain the coefficients

$$c(k^{(0)}, k^{(j)}) = \delta_{2^T k^{(0)} + 2^{T-j} k^{(j)}, 0} + \varepsilon c^{(1)}(k^{(0)}, k^{(j)}) + O(\varepsilon^2) \tag{3.41}$$

where

$$\begin{aligned} c^{(1)}(k^{(0)}, k^{(j)}) &= -i(2^j k^{(0)} + k^{(j)}) \sum_{\nu=0}^{\infty} 2^\nu [G_{2^{\nu+1}(2^j k^{(0)} + k^{(j)})} + G_{2^{T+\nu+1}(2^j k^{(0)} + k^{(j)})}] \\ &- i2^{(j-1)} [G_{(2^j k^{(0)} + k^{(j)})} + G_{2^T (2^j k^{(0)} + k^{(j)})}] \\ &- ik^{(0)} \sum_{\nu=0}^{j-2} 2^\nu [G_{2^{\nu+1}(k^{(0)} + 2^{-j} k^{(j)})} \delta_{k^{(j)}, 2^{j-\nu-1} m} + G_{-2^{T+\nu+1}(k^{(0)} + 2^{-j} k^{(j)})}] \end{aligned} \tag{3.42}$$

One should also expect that the two dimensional projections converge towards an asymptotic form in the limit of large delay.

3.4.2 Results for a particular form of feedback

For ease of presentation and in order to clarify our ideas let us first consider a particular choice for the function g in Eq. (3.21), namely

$$g(\varphi) = \varphi(\pi - \varphi) \quad \text{for} \quad \varphi \in [0, \pi], \qquad g(\varphi) = g(\varphi + \pi) \quad . \tag{3.43}$$

The Fourier coefficients of this function are

$$G_{2k} = \frac{-2}{(2k)^2}, \qquad G_{2k+1} = 0 \quad \forall \quad k. \tag{3.44}$$

With Eq. (3.44) in Eqs. (3.40) and (3.39), we have the first order approximation for the coefficients

$$c^{(1)}(k^{(0)}) = \frac{i}{k^{(0)}}(1 + \frac{1}{2^{2T}}) \tag{3.45}$$

and for the one dimensional projection of the invariant measure:

$$\rho(\phi^{(0)}) = 1 - \varepsilon(1 + \frac{1}{2^{2T}})(\pi - \phi) + O(\varepsilon^2). \tag{3.46}$$

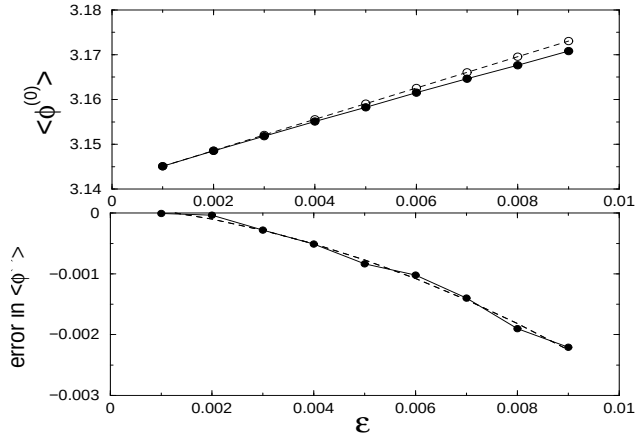

Figure 3.5: Above: $< \phi^{(0)} >$ as function of ε for $T = 2$; open circles correspond to the first order approximation and the closed ones to numerics. Below: difference between first order and numerics; the dashed line is a fit to a parabola, showing that the error is of second order in ε.

It is easy to see that this projection converges smoothly towards an asymptotic form.

We can check numerically the range of validity of our approximation observing the behaviour of the averages with respect to the invariant measure $< \phi^{(0)} >, < \cos(\phi^{(0)}) >, < \sin(\phi^{(0)}) >$. In order to give the average of the angle a definite meaning we have restricted the values of the angle to the interval $[0, 2\pi)$. In figures 3.5 and 3.6 some numerical results are compared to the first order approximation as a function of the coupling ϵ. All the numerical results clearly confirm that our approximations correctly describe the lowest order effects, and that the neglected higher order corrections lead to less than 10% effects for $\epsilon < 0.01$. In order to demonstrate that our results are to some extent uniform in the delay time we investigate the error for finite coupling ϵ in dependence on the delay time. The result displayed in figure 3.7 shows that the difference stays finite even if the delay becomes large. Such finding demonstrates that our expansion can be used even for large delay times.

Also the specific expressions for the two dimensional projections may be

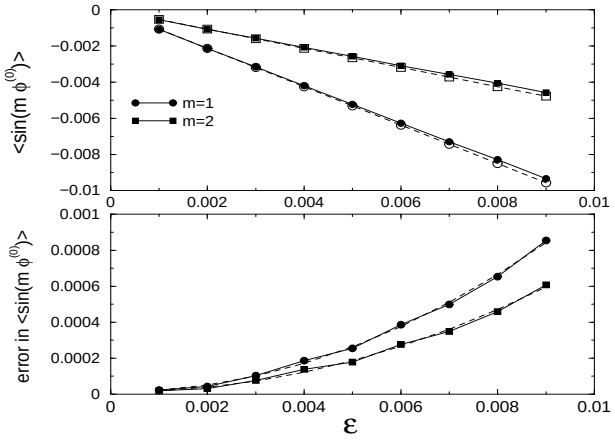

Figure 3.6: Similar to figure 3.5, with averages of $< \sin(m\phi^{(0)}) >$, which are related to the values of the coefficients $c(m)$. In the upper panel the closed symbols correspond to the first order approximation and the open ones to numerics. In the lower panel the difference between the first oder approximation and the numerics is depicted. The fit to a parabola shows that the error is of second order.

obtained.

$$\rho(\phi^{(0)}, \phi^{(j)}) = \delta(\phi^{(0)} - 2^{-j}\phi^{(j)}) + \epsilon \sum_{k^{(0)},k^{(j)}} c^{(1)}(k^{(0)}, k^{(j)}) e^{(k^{(0)}\phi^{(0)} + k^{(j)}\phi^{(j)})} \tag{3.47}$$

with j:

$$\begin{aligned} c^{(1)}(k^{(0)}, k^{(j)}) &= \frac{i}{2(k^{(0)} + 2^{-j}k^{(j)})}(1 + \frac{1}{2^{2T}}) + \frac{2^j i k^{(0)}}{(2^j k^{(0)} + k^{(j)})^2}(\delta_{k^{(j)},2m} + \frac{1}{2^{2T}}) \\ &+ \frac{2ik^{(0)}}{4(k^{(0)} + 2^{-j}k^{(j)})^2} \sum_{\nu=0}^{j-2} 2^{-\nu}(\delta_{k^{(j)},2^{j-\nu}n} + \frac{1}{2^{2T}}) \end{aligned} \tag{3.48}$$

where m and n are integers.

We can see that also the two dimensional projections of the invariant density will have an asymptotic form for large T and that the convergence rate in this limit will also be proportional to 4^{-T}. In figures 3.8–3.9 we show some comparison between this approximation and numerical results.

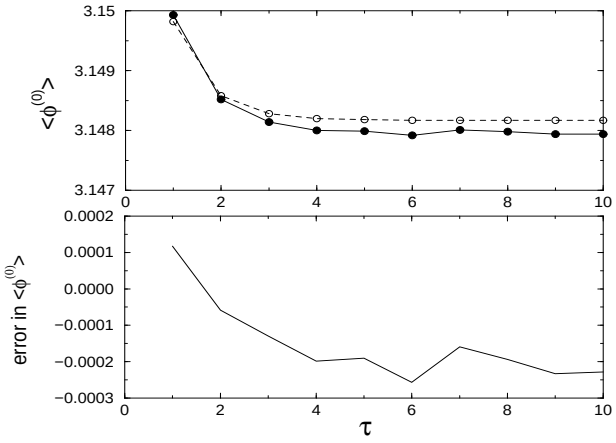

Figure 3.7: Above: $< \phi^{(0)} >$ as function of T for $\varepsilon = 0.002$, open closed circles have same meaning as in previous figures. Below: the difference between the first order approximation and numerics is depicted.

Because of numerical fluctuations of the averages the quadratic dependence of the error on ε is hardly visible here.

In order to check if the arguments of section 3.3 apply here, we should investigate the correlation function for small ϵ. A superficial inspection of Eq. (3.47) suggests that to leading nonvanishing order correlations between $\phi^{(0)}$ and $\phi^{(T)}$ decay as 2^{-T}. That rate apparently differs from the convergence rate of the one particle density which according to Eq. (3.46) is given by 4^{-T}. Thus one has to clarify how the decay of correlations is related to the convergence properties for large delays. For that purpose let us have a look at perturbative result (3.40). If the delay term is Hölder continuous of order ℓ then its Fourier coefficients decay like $G_k \sim k^{-\ell-1}$ and Eq.(3.40) tells us that the one particle density converges according to a power law $2^{-(\ell+1)T}$. If g is analytic then Fourier coefficients decay even faster, namely exponentially $G_k \sim \exp(-\alpha k)$ and the convergence of the one particle density is hyperexponential $\exp(-\alpha 2^{-T})$. Thus the mixing rate of the map together with the analytical properties of the delay term determine the convergence rate of the projected measure. In fact the correct convergence rate is reflected by a suitable correlation function, namely the pair correlation of $g(\phi)$ itself, which can be easily computed taking the Fourier series into account.

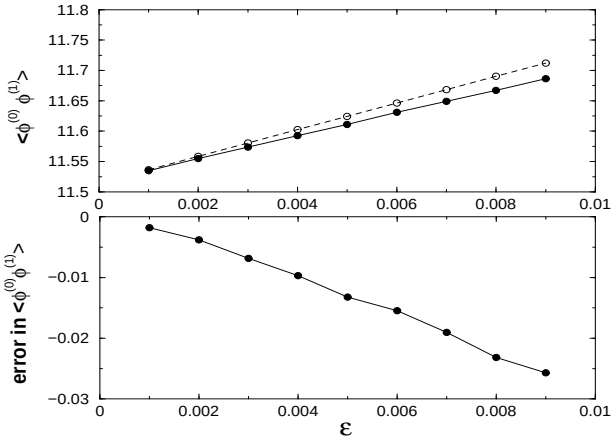

Figure 3.8: Above: $< \phi^{(0)}\phi^{(1)} >$ as function of ε for $T = 2$; open circles correspond to the first order approximation and the closed ones to numerics. Below: difference between first order and numerics.

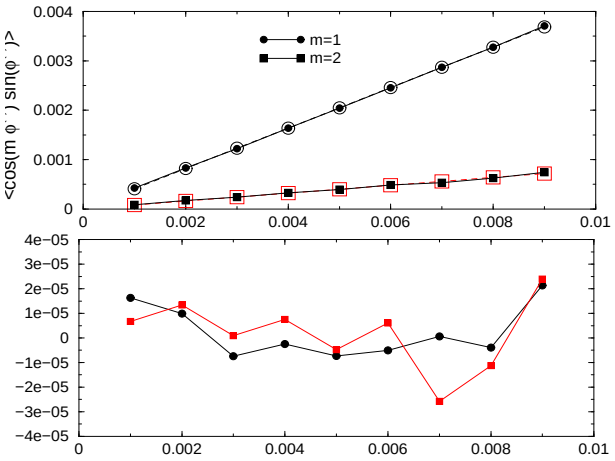

Figure 3.9: Upper panel: Averages of $< \cos(m\phi^{(0)})\sin(\phi^{(1)}) >$ for $T = 2$, which are related to the values of the coefficients $c(m, 1)$. The closed symbols correspond to the first order approximation and the open ones to numerics. Lower panel: Difference between numerical results and first order approximation.

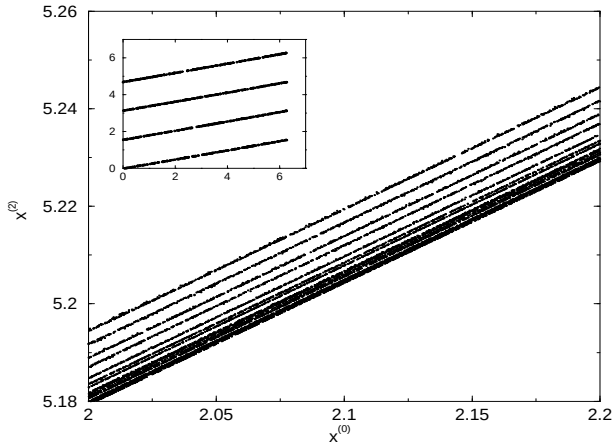

Figure 3.10: Part of projection of the attractor of Eq.(3.21) with $\varepsilon = 0.01$ and $T = 5$, on the plane $\{x^{(0)}, x^{(2)}\}$. Part of one strip is shown while in the inset the whole projection can be seen. At larger delays (and small enough ε) the strips are preserved but the structure inside them smooths out. The thickness of the strips is observed to be of the order of ε.

Although we have restricted our analysis to first order in ε we expect that higher order contributions will have the same qualitative behaviour, at least regarding the one dimensional projection. In order to make this study more complete, we have reproduced the numerical analysis of figures 3.3 and 3.4 in the case of map (3.21). As it can be seen from the lower panel of figure 3.11, the one dimensional projection converges also when ϵ is large. The convergence is smooth and the discrepancy between the measure at low and large delays depends on ϵ similarly as the first order approximation suggests.

3.5 What have we learned about the densities?

We have analysed the limit of large delay in a particular time discrete system by an analytical perturbation expansion. The validity of the expansion has been confirmed by numerical simulations. Our result shows that projected measures converge in the limit of large delay, where the rate of convergence is determined by the mixing rate of the chaotic map and by analytic properties of the delay term. Chaos plays of course an important role for the

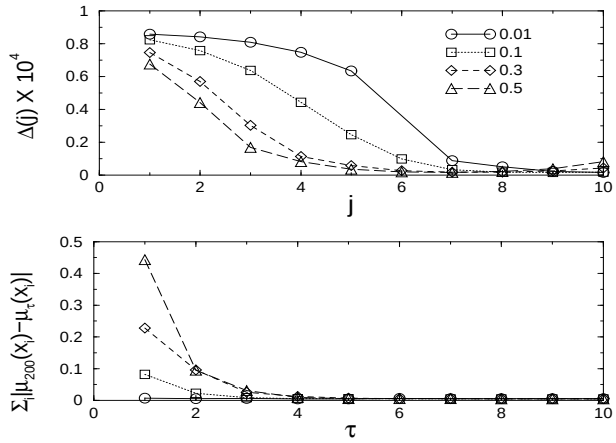

Figure 3.11: $\Delta(x_n, x_{n-j})$ (upper panel) and the average difference between measures at low and large delay (lower panel) for the map (3.21).

convergence since otherwise correlations would not decay and smooth densities would not exist in general. However, it is not the plain mixing rate which is responsible for the rate of the convergence but a particular pair correlation which involves the analytical properties of the delay term.

Our treatment was confined to a first order expansion. But we have good indications that our results are valid beyond such an order and we suppose that one might even be able to perform a formal proof of our statements along these lines. In addition, using e.g. diagrammatic or projection techniques it should be possible to go beyond our simple perturbative treatment. But such advanced approaches go far beyond the scope of this present work. Analytic approaches so far are restricted to hyperbolic systems, i.e. essentially to maps on the torus. Maps on intervals, e.g. even the simple Bernoulli shift (3.15) lacks such a treatment till today. Nevertheless numerical simulations indicate that qualitatively such models behave similarly.

Chapter 4

Why entropy does not grow?

4.1 Entropies of delayed systems

An intriguing fact observed numerically in many different scalar delayed systems is that in the large delay limit, when the dimension (estimated using the Kaplan-Yorke conjecture [37, 21]) of the attractors grow almost linearly as the delay increases, the entropy (estimated from Pesin's identity (see e.g. in [38]) remains practically unchanged (see figure 1.2 for an example). At a first glance this fact is counterintuitive: From one side as the delay increases, more degrees of freedom become unstable what is to be associated with more disordered motion, but the entropy does not grow, approaching an asymptotic value. This observation is even more puzzling if one considers that delayed maps can be represented as spatially extended systems as we will discuss in chapter 5. For spatially extended systems, it is well known that both dimensions and entropies are extensive quantities, i.e. they grow linearly with the size of the system, which in case of delayed systems corresponds to the delay value. The figure 4.1 illustrates this appearant contradiction.

Looking at the Lyapunov spectra one may have a quick answer to the question above: As the delay T increases more exponents become positive, but their absolute values decay like T^{-1}(c.f. figure 1.1 for an example). The two effects compensate each other and the entropy, which is estimated by the sum of positive Lyapunov exponents, does not grow. If one is satisfied with this answer it is not necessary to read further this chapter.

This chapter treats the issue above in a deeper way. What was sought here was to understand better the reasons why the entropy remains bounded

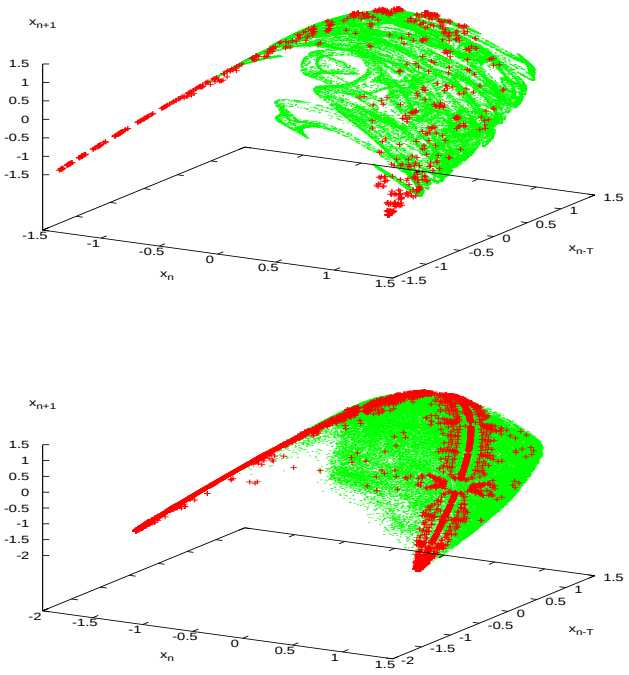

Figure 4.1: Projection of the attractor and the unstable periodic orbits on the subspace $(\{x_{n+1}, x_n, x_{n-T}\})$. When $T = 5$ (upper panel) $d_{KY} = 2.11$, $h_{KS} = 0.153$ while and when $T = 10$ (lower panel) $d_{KY} = 3.32$ and $h_{KS} = 0.119$.

at large delay. We have asked first if the topological entropy is also bounded at large delay and second what mechanism is responsible for bounded entropies from an information theory point of view. By investigating these aspects some intuition was gained about the large delay limit and the complexity of the system in that limit.

4.2 Some concepts on entropies

Before treating entropies of delayed maps, we make a small detour and present briefly some definitions and concepts related to the thermodynamic formalism of dynamical systems. This section is thus not necessary to further

understand this chapter if there is familiarity with the concepts presented.

Symbolic dynamics

The statistical description of mappings requires a partition of the phase space into subsets. Given an appropriate partition, one can analyse the chaotic motion through symbol sequences in a course-grained way.

The easiest way to partition a d-dimensional phase space X is to choose d-dimensional cubes of equal edge size δ. These cubes, usually called boxes in the literature, are labelled by an index i running from 1 to R where R is the total number of boxes. The boxes are non overlapping and cover the entire phase space. More generally, a partition $\{A\}$ is defined through cells A_i of different sizes and different shapes that are disjoint and cover the whole phase space, i.e.:

$$A_i \bigcap A_j = 0 \qquad \forall i,j \qquad i \neq j$$

and

$$\bigcup_{i=1}^{R} A_i = X.$$

A partition containing a fixed number of cells R of fixed size is generating if the infinite symbol sequence $i_0, i_1, i_2...$ uniquely determines the initial value x_0. To prove the existence and finding a generating partition is a very difficult task, with construction methods only known for one dimensional [39] or two dimensional [29] maps . Hence, for practical purposes, the partition in boxes is used. In the limit $\delta \to 0$ ($R \to \infty$), such a partition mimics a generating one.

Iterating a dynamical system, say a map f with initial condition x_0 belonging to a cell i_0 will produce a sequence of points $x_1, x_2, ...$ belonging respectively to cells $i_1, i_2, ...$ By this method it is possible to attribute to each initial value x_0 a symbol sequence that describes the trajectory in a coarse grained way. Each initial value x_0 generates an infinite symbol sequence and for a given finite symbol sequence $i_0, i_1, i_2, ...$ of length N one can identify a set o initial values denoted by $J[i_0, i_1, .., i_{m-1}]$ that generate this sequence. This set is called $m - cylinder$. The volume of such sets diminishes exponentially as m increases, i.e. the longer the sequence, the more precision on has in identifying the region to which the corresponding initial condition belongs. If the sequence is forbidden the corresponding cylinder is empty. The rules that determine the forbidden sequences are known as pruning rules and determine a "grammar" of a dynamical system.

These rules will define the topological properties and therefore are intimately related to periodic orbits (see e.g. in [33]).

Some sequences will appear more frequently than others. Hence it is possible to attribute to each sequence, a probability $p(i_0, i_1, i_2, ..., i_m)$ to be observed. This probability is related to a probability density $\rho(x_0)$ of initial conditions:

$$p(i_0, i_1, i_2, ..., i_N) = \mu(J[i_0, i_1, ..., i_m]) \tag{4.1}$$

where

$$\mu(J[i_0, i_1, ...]) = \int_{J[i_0, i_1, ..., i_m]} dx_0 \rho(x_0). \tag{4.2}$$

A natural choice for this distribution is the invariant density of the systems (consequently $\mu(J[i_0, i_1, ..., i_m])$ is the natural invariant measure) which produces stationary probabilities. Other choices could be made however (for instance a density based in the unstable periodic orbits [34]).

The hierarchy of all probabilities $p(i_0, i_1, i_2, ..., i_N)$ with $N = 0, 1, 2, ...$ defines a stochastic process and one can always write the probability of a given sequence as:

$$p(i_0, i_1, i_2, ..., i_m) = p(i_m | i_0, i_1, i_2, ..., i_{m-1}) p(i_0, i_1, i_2, ..., i_{m-1}) \tag{4.3}$$

where the conditional probability

$$p(i_m | i_0, i_1, i_2, ..., i_{m-1}) = \frac{p(i_0, i_1, i_2, ..., i_{m-1})}{p(i_0, i_1, i_2, ..., i_m)} \tag{4.4}$$

is the probability of i_m provided that the history $i_0, i_1, i_2, ..., i_{m-1}$ has happened. The symbolic stochastic process will define a Markov chain if

$$p(i_m | i_0, i_1, i_2, ..., i_{m-1}) = p(i_m | i_{m-1}) \tag{4.5}$$

i.e., the conditional probability only depends on the last event and not on all past history. Another simple stochastic process is a topological Markov chain, defined by the property:

$$p(i_m | i_0, i_1, i_2, ..., i_{m-1}) = 0 \tag{4.6}$$

if and only if $p(i_m | i_{m-1}) = 0$ or $p(i_{m-1} | i_0, i_1, i_2, ..., i_{m-2}) = 0$. Special dynamical systems may possess the properties (4.5) or (4.6) if the partition is chosen properly (if a Markov partition can be found), but in general the stochastic process related to a dynamical system will be a complex non Markovian process.

The Rényi entropies

The Rényi entropies, like the Shannon entropy, characterise a probability density p_i. They are defined by:

$$H_\beta = \frac{1}{1-\beta} \ln \sum p_i^\beta \tag{4.7}$$

and are information measures like the Shannon entropy (in fact the Shannon entropy is recovered in the limit $\beta \to 1$). This definition can be applied to dynamical systems and in this case, p_i are the probabilities of the different sequences to occur.

From now on we will make statistics on sequences and therefore, it is useful to limit ourselves to allowed sequences, i.e. sequences whose probability is nonzero. We denote the total number of allowed sequences of size m , $\omega(m)$ and label the probability of a particular sequence of this size as $p_j^{(m)}$ (the index j runs therefore from 1 to $\omega(m)$.

In the context of dynamical systems, the Rényi entropies are defined by

$$h_\beta = \sup_{\{A\}} \lim_{m\to\infty} \frac{1}{m} \frac{1}{1-\beta} \ln Z_m(\beta) \tag{4.8}$$

where $Z_m(\beta)$ is the dynamical partition function:

$$Z_m(\beta) = \Sigma_{j=1}^{\omega(m)} (p_j^{(m)})^\beta. \tag{4.9}$$

The exponent β is the order of the entropy and will control the emphasis that is given to sequences with small or large probabilities: the larger the value of β the more weight have the sequences with large probability. By varying β one can span a whole spectrum of entropies. Here, this will not be discussed further, but instead we concentrate on the three integer values of β giving rise to the entropies studied in this work.

The idea of finding all possible partitions and then looking for the one that maximises (4.8) is rather cumbersome. The situation becomes better if a generating partition is known but since this is true only for very special cases the usual procedure is to construct a partition using boxes and making their sizes tend to zero. In this context, the Rényi entropies are defined as:

$$h_\beta = \lim_{\delta\to 0} \lim_{m\to\infty} \frac{1}{m} \frac{1}{1-\beta} \ln Z_m(\beta) \tag{4.10}$$

Topological entropy.

The zeta function for for $\beta = 0$ just gives the total number of allowed symbol sequences of length m. For very large m it is possible to write:

$$\omega(m) \sim e^{mh_0} \tag{4.11}$$

and therefore, h_0 describes the growth rate of the number of allowed symbol sequences with m, also known as the topological entropy (to be denoted h_{TOP} in the rest of this work).

From the concept of partitions it is possible to define a transition matrix T such that T_{ij} is 1 if the transition from cell A_i to A_j is allowed and 0 otherwise. Thus, the product T^m is related to all possible symbol sequences of length m. The sum of all elements of T^m gives, therefore, $\omega(m)$, and the logarithm of the largest eigenvalue of T^m gives the topological entropy in the limit $m \to \infty$ [33]. In the case of some expanding maps, it is usually possible to find a partition, such that a finite dimensional matrix T describes the dynamics and the topological entropy might be obtained analytically as described above. Such cases correspond to subschifts of finite type, i.e. mappings whose pruning rules can be truncated at a finite period. This is not at all the general case and an alternative way to estimate the topological entropy is necessary.

The growing rate of $\ln[\omega(m)]/m$ is well approximated by the growing rate $\ln[TrT^m]/m$, i.e. one can use the trace of T^m to estimate the topological entropy. Since the trace gives the number of sequences that return to the same element after m interactions, it is exactly the number of periodic points of period m [1]. Hence, in the limit $m \to \infty$, the the topological entropy can be estimated by [40],[39]:

$$h_{top} = \limsup_{m\to\infty} \frac{\ln N(m)}{m} \quad . \tag{4.12}$$

This is only an estimate if the pruning rules are not known for all periods.

For one dimensional mappings ($x_{n+1} = f(x_n)$) another way to estimate the topological entropy exists using the number of pre-images of $y = f^m(x)$. Calling this number $N(m)$, Eq. (4.12) is recovered for the entropy [39]. This method is also based on the idea of a transition matrix.

[1] A periodic orbit of period p as defined in chapter 2 has p periodic points.

Kolmogorov-Sinai entropy

In the limit $\beta \to 1$ the Kolmogorov-Sinai entropy is obtained from Eq. (4.10). Considering the partition given by boxes of size δ, the Kolmogorov-Sinai entropy is defined as:

$$h_{KS} = h_1 = \lim_{\delta \to 0} \lim_{m \to \infty} \frac{1}{m} \Sigma_{j=1}^{\omega(m)} p_j^{(m)} \ln p_j^{(m)} \tag{4.13}$$

if a general partition $\{A\}$ is to be considered, the supremum must be taken just as in 4.8.

The KS entropy is a measure of how much information is gained (or lost) as the chaotic system evolves in time. This meaning becomes clearer when the block entropies are considered:

$$H_m = \Sigma_{j=1}^{\omega(m)} p_j^{(m)} \ln p_j^{(m)} \tag{4.14}$$

$$H_{m+1} = \Sigma_{j=1}^{\omega(m+1)} p_j^{(m+1)} \ln(p_j^{(m+1)}) \tag{4.15}$$

According to Shannon's ideas [41] H_m is a measure of the amount of information in the set of sequences with length m. The metric entropy measures how much information is gained in one step if all m past steps are known, in the limit of very long sequences, i.e. it can be defined by:

$$h_{KS} = lim_{\delta \to 0} lim_{m \to \infty} h(m) \tag{4.16}$$

with

$$h(m) = H_{m+1} - H_m. \tag{4.17}$$

The convergence of Eq. (4.16) is uniform from above, i.e.

$$h(m+1) \leqslant h(m) \tag{4.18}$$

what can be easily proved with the help of Eqs. (4.4) and (4.14).

Speaking more intuitively, chaotic systems create information in the following way: suppose a set of initial conditions is confined in one box of size δ and cannot be distinguished from each other (i.e. the resolution is restricted to δ). After one iterate, due to the expanding property, many boxes will be occupied and it will be possible to distinguish among initial conditions, without improving the resolution. This local expansion of initial conditions

is measured by the Lyapunov exponents and indeed, there is a relation between the Kolmogorv Sinai entropy and the Lyapunov exponents. It is the well know Pesin's inequality (see e.g. [38] for a formal statement):

$$h_{KS} \leqslant \Sigma_i \lambda_i^{(+)} \tag{4.19}$$

the equality holds if the invariant measure is smooth along the expanding directions.

A last important remark regarding the KS entropy is that it is a measure of "chaos" and unpredictability: The larger its value the more difficult it will be to guess, on the basis of the past history, the next outcome.

The correlation entropy

Another important quantity, is obtained with $\beta = 2$ in Eq. (4.10), the correlation entropy. This entropy is a lower bound to the metric and topological entropies, i.e.

$$h_2 \leqslant h_1 \leqslant h_0 \tag{4.20}$$

what follows from the more general consideration:

$$h_{\beta'} \leqslant h_\beta \qquad if \qquad \beta' \geqslant \beta. \tag{4.21}$$

The correlation entropy and the corresponding correlation dimension are the quantities usually computed when one wants to characterise chaotic motion from a time series. Thanks to a method derived in [21] it provides better statistics and requires less computational effort than computing the KS entropy from the invariant density. Having a time series with N state vectors $\{\vec{v}_n^m\}$, obtained by a m-dimensional delay embedding, the then correlation sum is given by:

$$C_2(m,\delta) = \frac{1}{N(N-1)} \Sigma_{i \neq j} \Theta(\delta - |\vec{v}_i^m - \vec{v}_j^m|). \tag{4.22}$$

from which the correlation dimension can be estimated by

$$D_2(m,\delta) = \frac{\partial \ln C_2(m,\delta)}{\partial \ln \delta} \tag{4.23}$$

as long as the embedding dimension m is large enough. To be strict one should consider Eq. (4.23) in the limit $N \to \infty$ and $\delta \to 0$ [21] in order to

recover a dimension. This is not possible in practice and instead of performing the limit, one looks for a region such that $D_2(m, \delta)$ is independent from δ.

Inside this scaling range, where the dimension is independent from δ, the correlation entropy can be obtained from:

$$h_2(m, \delta) = \ln \frac{C_2(m, \delta)}{C_2(m+1, \delta)} \tag{4.24}$$

which should converge to a constant if m is large enough. The length of the scaling range and how large must m be depends strongly on the system as discussed in [42]. This method will be used later, when we will estimate the correlation entropy of a time series generated by delayed systems.

4.3 Is the topological entropy bounded?

This section is devoted to discuss the behavior of topological entropy of delayed maps in the large delay limit. Addressing this issue was motivated by two facts: knowledge of the metric entropy estimated from Lyapunov exponents does not allow to make any inference about the topological entropy; and it would be interesting to investigate which topological properties are behind the boundedness of the entropy (if exists).

4.3.1 An answer from the cycles

Our first aim was to investigate the issues above for a general delayed map given by Eq. (1.4). The only approach that allowed this generality was to investigate the behavior of periodic orbits in the large delay limit, an issue already discussed in chapter 2. From section 2.2.1 we know that for any p, Eqs. (2.2), (2.3) are invariant under the transformation $T \mapsto T + np$, $n \in \mathbf{Z}$ of the delay value. Period-p orbits found for a delay value T will be exactly the same as those for $\tilde{T} = T + np$, as long as $\tilde{T}$ and T are both positive. As a consequence, one has the following relation for the p-periodic points of the map:

$$N(p, T) = N(p, T + np), \tag{4.25}$$

where $N(p, T)$ denotes the number of p-periodic points for a delay T.

We are going to use this relation to estimate the topological entropy of the map (1.4). As a consequence of Eqs. (4.25) and (4.12), we derive an

heuristic argument, why the topological entropy should be bounded in the limit of large delay. For a finite period p, we have the relation

$$N(p,T) = C(p,T)\exp[ph(T)] \tag{4.26}$$

where in view of Eq.(4.12) the pre-factor obeys the constraint

$$\limsup_{p\to\infty} \frac{\ln C(p,T)}{p} = 0 \tag{4.27}$$

i.e. it depends on p weaker than exponentially. If we combine Eq.(4.26) and Eq.(4.25) we get the exact equations

$$\begin{aligned} C(p,T)\exp[ph(T)] = N(p,T) = N(p,T+2p) = \\ C(p,T+2p)\exp[ph(T+2p)]. \end{aligned} \tag{4.28}$$

and

$$\begin{aligned} C(2p,T)\exp[2ph(T)] = N(2p,T) = N(2p,T+2p) = \\ C(2p,T+2p)\exp[2ph(T+2p)]. \end{aligned} \tag{4.29}$$

Therefore our final result can be written as:

$$\begin{aligned} h(T+2p) = h(T) + \frac{\ln C(2p,T) - \ln C(p,T)}{p} - \\ \frac{\ln C(2p,T+2p) - \ln C(p,T+2p)}{p}. \end{aligned} \tag{4.30}$$

If the third term in the R.H.S of Eq. (4.28) is bounded one should expect that in the limit $p \to \infty$, the entropy $h(\infty)$ is finite [2]. The figure 4.2 illustrates the argument in a more intuitive way.

All our previous expressions are valid for arbitrary T and p. In our final argument we have used the assumption that to some extent the limit (4.29) is uniform in the delay time. Such an assumption cannot be proven in the general case and we will have a closer look on this issue within the discussion of our examples. Nevertheless, under such a quite general assumption the topological entropy remains bounded in the limit of large delay time.

[2]The second therm in the R.H.S of Eq. (4.28) vanishes due to (4.29).

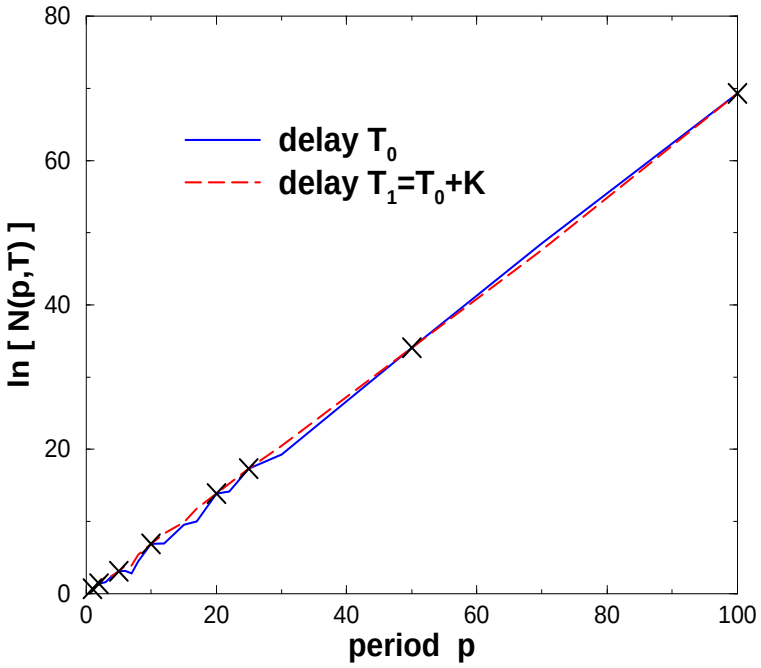

Figure 4.2: The crosses correspond to points common to both curves, i.e. points where p is a sub-multiple of K. If K is large and not prime (i.e. $K \to \infty$) there are many points in common at small and large periods. Hence also for $p \to \infty$ one should find points shared by both curves.

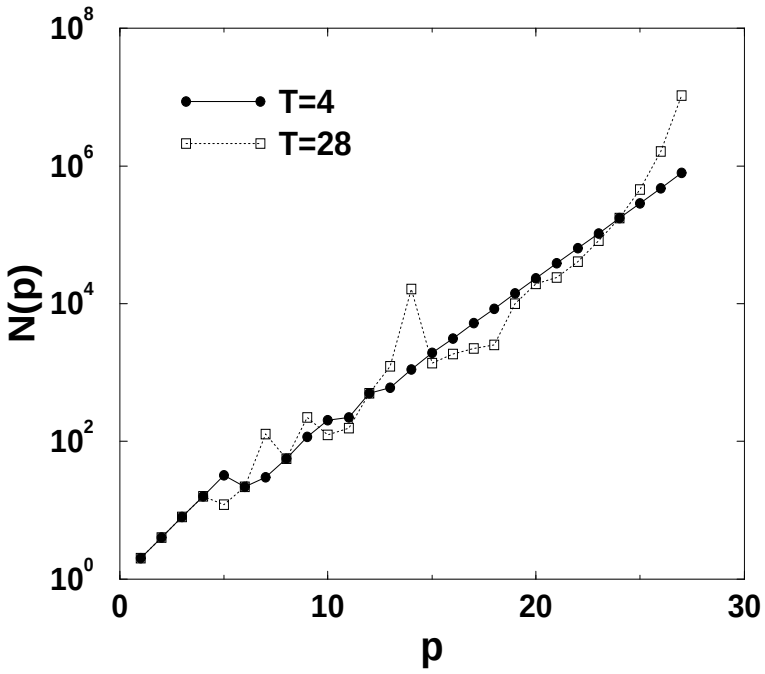

Figure 4.3: As a concrete example: For the Bernoulli map with $\varepsilon = 0.2$ the number of periodic points for two different delay values.

4.3.2 An answer from partitions

Investigating the periodic orbits we have gained an argument for the boundedness of topological entropy, but could not obtain more illuminating details, e.g. an upper bound for it or know the mechanism responsible for this boundedness. Such details are difficult to be obtained in a general way and therefore we restrict to a special type of delayed map [27]:

$$M : x_{n+1} = (1-\epsilon)F_1(x_n) + \epsilon F_2(x_{n-T}), \tag{4.31}$$

which mimics to some extend the coupling known from unidirectional coupled map lattices. Here the parameter ϵ governs the strength of the delay term. The special structure of Eq.(4.31) ensures that the dynamics is well defined irrespectively of the type of the particular map.

There are two simple cases where the topological entropy can be evaluated by inspection. First considering $\epsilon = 0$ the system turns out to be a one-dimensional map and the topological entropy is equal to that of the map F_1. In the opposite case, $\epsilon = 1$, Eq.(4.31) reduces to $T+1$ independent copies of the map F_2 acting on the time scale $T+1$. Hence, if $N(k,0)$ denotes the number of period–k points of the map F, then by combinatorics (4.31) with $\epsilon = 1$ has $N(p,T) = N(k,0)^{T+1}$ periodic points of period $p = k(T+1)$. Taking the limit $k \to \infty$ equation (4.12) yields again the topological entropy, per unit time, of the single map F_1 or F_2.

For intermediate values of ϵ no general reasoning seems to be available but we can speculate :

$$h_{top}(M) \leqslant sup\{h(F_1), h(F_2)\} \tag{4.32}$$

on the basis of the reasoning that for $\epsilon \neq 0$ or 1 one has more severe pruning rules. This idea is supported by numerical results of [27], showing that the metric entropy has a minimum for some $\epsilon \in (0,1)$, and by our computations of the topological entropy to be shown in the next section.

One can establish a rigorous upper bound for the topological entropy if the functions F_1 and F_2 are piecewise linear. Consider that they satisfy this condition, act on an interval I and are linear in R sub-intervals. This property defines automatically a generating partition with R elements, and therefore, the maximal allowed value for the topological entropy will be

$$h_{top} \leqslant \ln(R). \tag{4.33}$$

This situation gives a more insightful understanding: the number of elements of the generating partition, in this case, is not affected by changing

the delay value [3]. This argument gives naturally an upper bound for the topological entropy, namely the logarithm of the number of elements of the partition. One should be aware, however, that the grammar (the pruning rules governing the existence or not of a given sequence) changes as the delay varies. The pruning always reduces the entropy and we cannot estimate its value from these arguments.

4.3.3 Examples: Some specific maps.

Bernoulli shift

As a first example, we consider the map of Eq. (4.31) with

$$F(x) = 2x - \mathrm{sgn}(x), \quad x \in [-1, 1]. \tag{4.34}$$

Since the map is piecewise linear its periodic points can be easily estimated as consequence of the existence of generating partition. Consider an orbit of period p, $\overline{x}_0$, $\overline{x}_1$, ..., $\overline{x}_{p-1}$. Then by $\sigma_k := \mathrm{sgn}(\overline{x}_k)$ we can assign a period–p symbol sequence to this orbit. This assignment is injective, i.e. there exists at most one period–p orbit for each period–p symbol sequence: Combining Eq.(4.31) and Eq.(4.34) the periodic orbit is determined by

$$\overline{x}_{n+1} = 2(1-\epsilon)\overline{x}_n + \epsilon\overline{x}_{n-T} - (1-\epsilon)\sigma_n - \epsilon\sigma_{n-T} \tag{4.35}$$

and such a linear inhomogeneous equation has at most one solution which satisfies the self consistency condition $\mathrm{sgn}(\overline{x}_k) = \sigma_k$ for a given symbol sequence σ_0, σ_1, ..., σ_{p-1}. Hence the number of period–p points obeys

$$N(p, T) \leqslant 2^p \tag{4.36}$$

and the topological entropy of the single map F yields an upper bound for the entropy of the map.

In the figure 4.4 we compare numerically obtained values of the topological entropy and the Kolmogorov Sinai entropy for $T = 1$ and different values of ϵ. For this particular model the exact values of both entropies coincide since the Jacobian is constant. A proof for this statement is based on the absence of multifractality in the system i.e. all the Rényi entropies can be shown to have the same value. Thus the difference visible in figure

[3] Another way to see this is remembering that the number of pre-images of a given point is not affected by the delay value. In this sense, some arguments of 1 dimensional maps [39] apply here although the maps are higher dimensional.

4.4 yields the accuracy for the method by which the topological entropy was estimated. Apart from deviations near the minimum the topological entropy was accurately recovered. In fact near such a minimum we expect quite dramatic topological changes that prevent a good convergence of the estimates of h_{top} based on Eq. (4). This minimum appears also for higher delay values (see figure 4.5). The exact location of the minimum approaches $\epsilon = 0.5$ in the limit $T \to \infty$ [27], when the curve of the entropy is symmetric in respect to this point, although the one for the dimension is similar to that shown in 4.5.

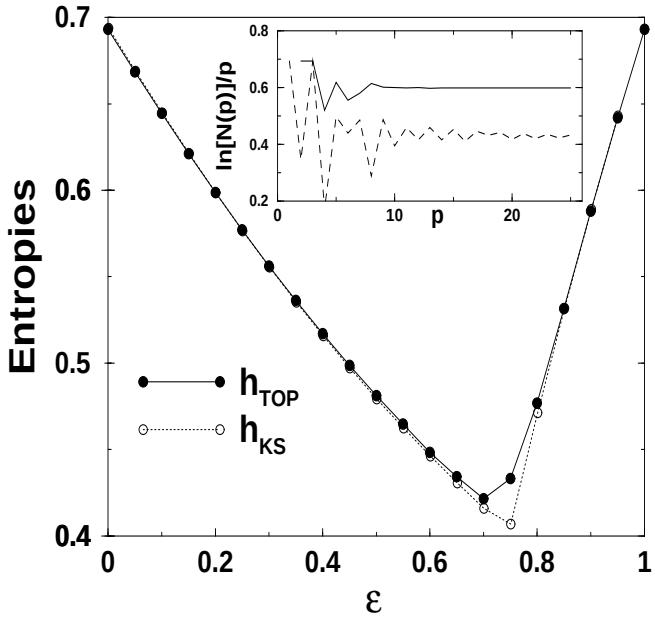

Figure 4.4: Estimated topological and metric entropies (h_{top} and h_{ks} respectively) for the Bernoulli shift with $T = 1$. Metric entropies have been estimated from the Lyapunov spectrum using Pesin's identity and topological entropy by $\ln N(p, 1)/p$ with $p = 25$. The inset shows the estimates of topological entropy as a function of the period for $\epsilon = 0.2$ (solid line) and $\epsilon = 0.75$ (dashed line).

A slightly more detailed analysis is possible based on a numerical evaluation of Eq.(4.35). Here a severe kind of pruning can be detected which is related to the time scale set by the delay T. First of all, if we consider pe-

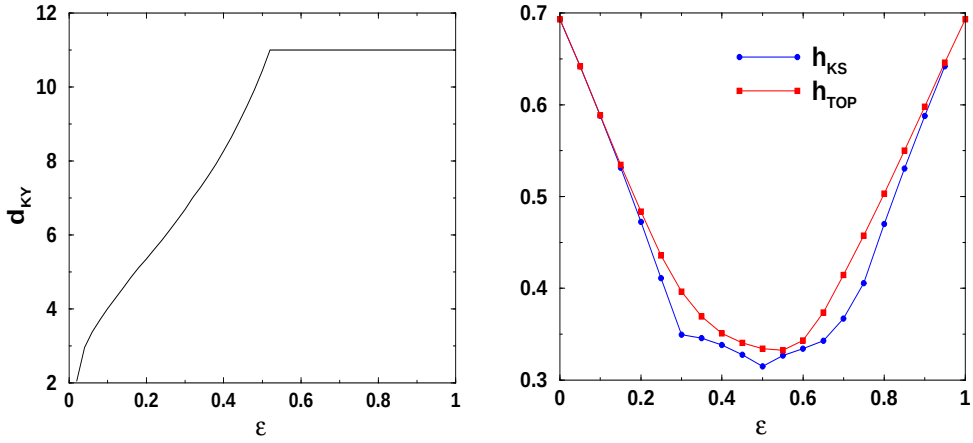

Figure 4.5: Dimension and entropies for the Bernoulli map with $T = 10$ as a function of ϵ. The topological entropy was estimated with $\ln N(p, 10)/p$ with $p = 27$. The difference between h_{KS} estimated from Pesin's identity and the topological entropy estimated from the orbits is due to lack of precision in the second one.

riodic points of period $p = T$, then because of $\overline{x}_{n-T} = \overline{x}_n$ Eq.(4.31) reduces to the single map F. Hence the delayed system admits the same number of periodic points of order $p = T$ as the single map F. A similar feature occurs for periods $p = T + 1$. Here because of $\overline{x}_{n-T} = \overline{x}_{n+1}$ Eq.(4.35) reduces to

$$0 \leqslant |x_n| = \frac{1}{2}(1 + \sigma_n\sigma_{n+1}) + \frac{1 - 2\epsilon}{2(1 - \epsilon)}(-\sigma_n\sigma_{n+1})(1 - |x_{n+1}|). \qquad (4.37)$$

Except for the fixed points the product $\sigma_n\sigma_{n+1}$ takes the value -1 for at least one n and the condition (4.37) is violated if $\epsilon > 1/2$. Otherwise, if $\epsilon < 1/2$ then Eq.(4.37) yields a contraction on $[0, 1]$ so that all symbol sequences are allowed. Hence if p is a prime factor of $T + 1$ then no prime orbit of period p appears if $\epsilon > 1/2$ but all prime orbits of period p appear if $\epsilon < 1/2$. Therefore, pruning rules depend sensitively on the fine tuning of the coefficients of the delay term. Fortunately these features do not corrupt the upper bound for the topological entropy, but an accurate estimation of the entropy from counting periodic orbits seems to be difficult. In the figure 4.6 these pruning rules can be seen in the case of $T = 11$.

The analysis carried out above shows that, just like in the delayed Hénon map, the Bernoulli shift has special periods of the order of T and which will

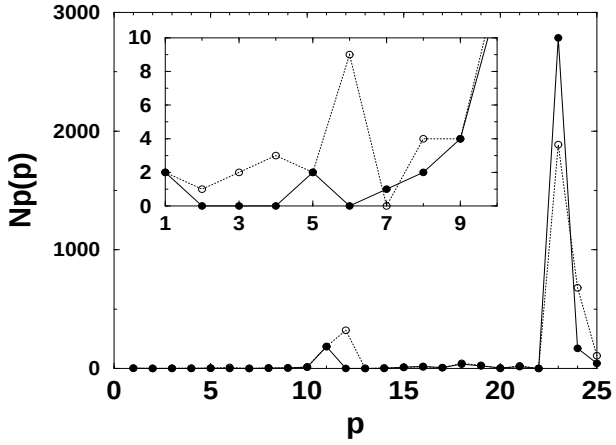

Figure 4.6: Number of prime orbits as a function of the period - $N(p,T)$ - for the map with Bernoulli shift for $T = 11$, $\epsilon = 0.45$ and $\epsilon = 0.5$ (empty and filled circles respectively).

have an impact in the convergence properties of the topological entropy, i.e. we should not expect a good estimate the topological entropy using Eq. (4.12) with period $p < T$. Details about this convergence is shown in figure 4.7.

Lozi

Another example of piecewise linear map we have chosen is similar to the Lozi map:

$$x_{n+1} = (1-\epsilon)(2 - 2x_n\sigma_n) + \epsilon x_{n-T} \tag{4.38}$$

with $\sigma_n := \mathrm{sgn}(x_n)$.

We perform the same calculations described for the Bernoulli shift in order to estimate the topological entropy of Eq. (4.38) from its periodic orbits. In this case, there is no minimum but the entropy decays as ϵ increases from 0 to 1 (c.f. figure 4.8)

Also for this map, special pruning rules are obtained for orbits with periods around the delay value. First, if $p = T$ one has $\overline{x}_{k-T} = \overline{x}_k$ and these orbits are given by the equations:

$$\overline{x}_{k+1} = (1-\epsilon)(1 - 2\overline{x}_k \mathrm{sgn}(\overline{x}_k)) + \epsilon \overline{x}_k. \tag{4.39}$$

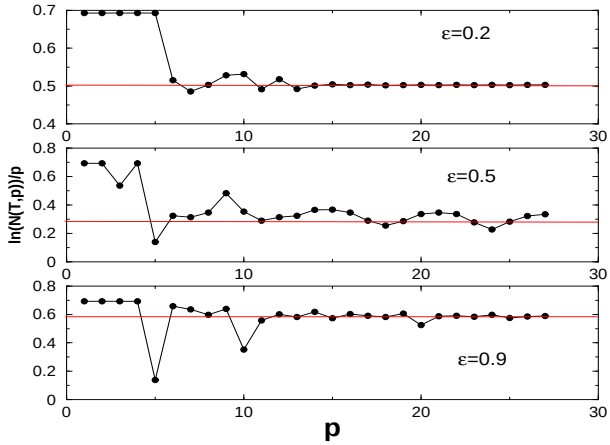

Figure 4.7: Estimates of topological entropy from periodic orbits for the Bernoulli map with $T = 4$. Convergence is reached only if $p > T$ and for $\epsilon \approx 0$ or 1.

A more interesting situation happens for $p = T+1$, in this case $\overline{x}_{k-T} = \overline{x}_{k+1}$, the orbits are solutions of:

$$\overline{x}_{k+1} = 1 - 2\overline{x}_k \text{sgn}(\overline{x}_k) \tag{4.40}$$

and $N(p, T) = 2^p$. In figures 4.9 it is possible to observe that the existence of these special periods will influence the convergence of the topological entropy also in this case, and good estimates are only obtained if $p > T + 1$ as in the other examples discussed here.

As long as conditions for convergence are satisfied, it is possible to obtain good estimates for the topological entropy for different delay values as depicted in figure 4.10. We see that the topological entropy estimated from the orbits is more or less constant with delay variation for a given ϵ value.

Hénon

Using the Biham-Wenzel method [28] to obtain the periodic orbtis and Eq.(4.12) we were able to obtain estimates of the topological entropy for the delayed Hénon map (Eq.(2.16)), which we show in figure 4.11 for different delay values. Comparing the estimated topological entropies with the metric entropies calculated from the Lyapunov exponents we observe that the values agree within the error bars. Although these results are limited

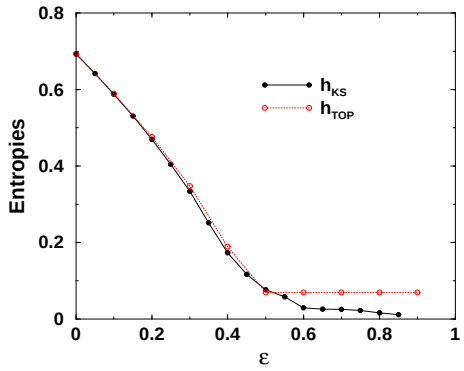

Figure 4.8: Dependency of the entropies on ϵ for the map (4.38) with $T = 5$. At the extrema of the interval $\epsilon = 0, 1$, the entropies are equal the one corresponding to the maps F_1 and F_2. Topological entropy was estimated with $\ln N(p, 1)/p$ with $p = 20$.

to relatively low delay values, they show an important property: the topological entropy agreed with the value of the corresponding metric entropy and moreover, its value does not grow as the delay grows but seems to be bounded. In that respect the model seems to share the properties of the Bernoulli system and Lozi map already discussed. It shows that our arguments can be valid also for a nonlinear map.

The error bars in figure 4.11 increase with the delay due to the convergence properties of the topological entropy. Estimates for the the topological entropy (full circles in figure 4.11) were obtained using the data sets containing the periods and the respective number of periodic points. Truncating the set at a given p, and fitting the data to Eq.(4.26), we obtained estimates for the entropy. Figure 4.12 shows how these estimates depend on p.

For the delay value $T = 6$ in figure 4.12 one can see a large peak for $p = T + 1$ oscillations around an average value for $p > T + 1$. The same pattern was observed for other low delay values as a consequence of the special periods discussed in section 2.2.4 c.f. Eq. (2.19). Therefore we can expect satisfactory convergence of the topological entropy only for $p > T + 1$. The results in figure 4.11 were obtained by the average of all values $h(T, p)$ such that $p > T + 1$ and the error bars indicate the amplitude of the oscillations.

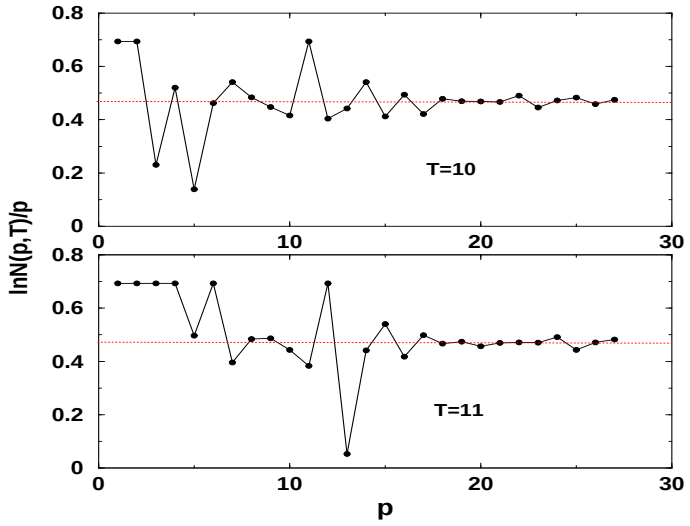

Figure 4.9: Estimates of the topological entropy of Eq. (4.38) with $\epsilon = 0.2$.The fluctuations with p are small, and the estimates of the entropy reach a nearly constant value only for for $p > T + 1$.

4.4 Why is there an asymptotic value?

This study would not be complete without a direct analysis of the metric entropy, without the need of Pesin's identity, and an explanation of its asymptotic behavior on the basis of metric properties. This section is devoted to this analysis. We present here the discussion of how the metric entropy could be estimated using a projection of the invariant density in a low dimensional subspace and how, as a consequence, this entropy has an asymptotic limit value.

4.4.1 First step: Estimating the entropies.

Following a logical thread from section 4.3, one would think that the periodic orbits would be the key to understand the behavior of any ergodic average in the large delay limit: Since the low period orbits reappear again and again as the delay increases, one could naively think that the measure obtained from them through cycle expansion methods (see e.g. [33]) would allow one to obtain also the metric entropy. The problem with this reasoning is that for such methods to converge (i.e. in order to obtain good estimates of

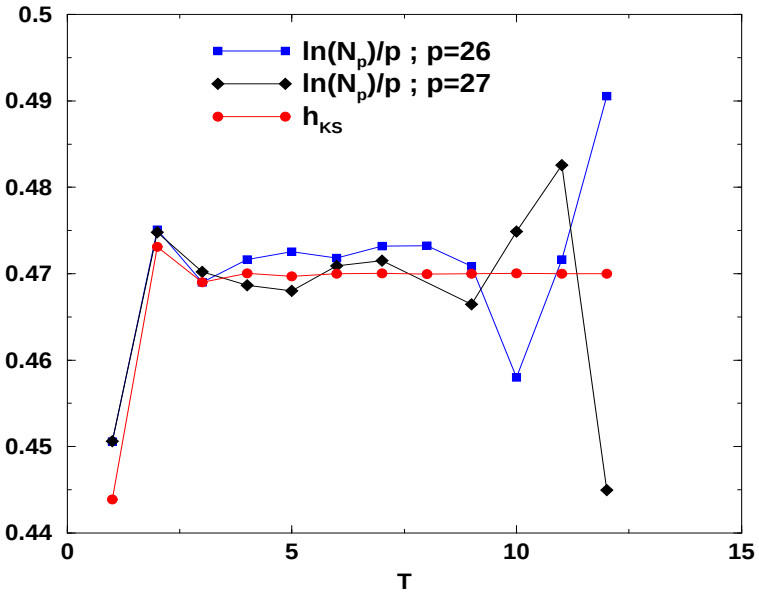

Figure 4.10: KS entropy estimated with Pesin's identity and estimates of topological entropy for the Lozi delayed map with $\epsilon = 0.2$. As the delay grow the estimates of the topological entropy become poorer (convergence is not achieved for periods $p = 26, 27$) but it is possible to see that the behavior of the two entropies are essentially the same with respect to increase of delay value.

the entropies) one needs to go to periods of the order of the delay value. Some hope would exist if one considers only periods of order kT, but even in simple cases, pruning rules for such periods are not evident and obtaining these rules numerically is very hard as the computation time to find the orbits grows exponentially with the period.

On the other hand, if one tries to construct the measure directly from a long trajectory and apply the definition (4.13) one realises that a huge numerical effort is necessary since Eq. (4.16) has bad convergence properties in the limit of large T, and the amount of data necessary to compute the probabilities is expected to grow exponentially as the dimension grows. Therefore, we have used an alternative way to estimate the metric entropies: Inspired by a method developed for coupled map lattices [43], we concentrate on subspaces of interest and use the projection on theses subspaces to estimate the entropy.

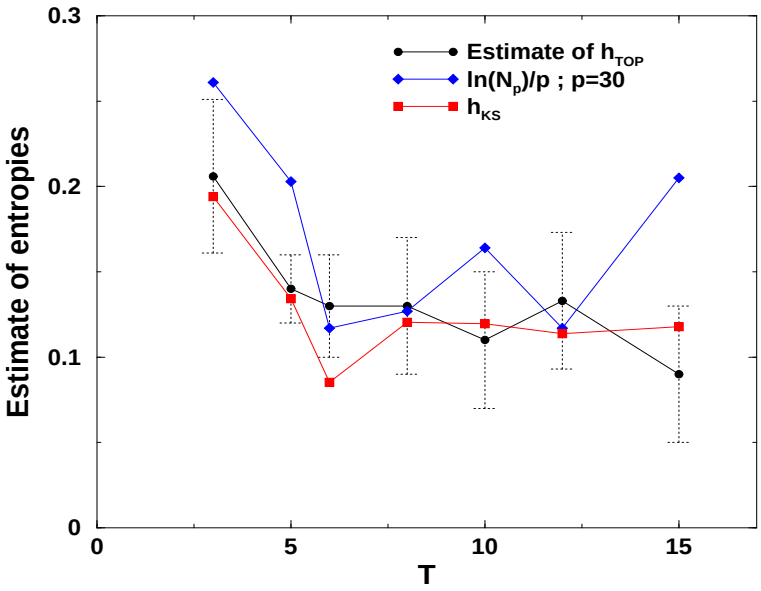

Figure 4.11: Estimates of topological and metric entropies of the model (2.16) with parameters $a = 1.0$ and $b = 0.3$. Metric entropies have been estimated from the Lyapunov spectrum using Pesin's identity. See text for a description of how h_{top}, denoted with full circles were obtained.

The central idea of the method consists in considering only a subspace of the high dimensional phase space $X_{\vec{s}}$, spanned by a state vector $\vec{s}$ partitioned in boxes of edge δ. Using the projection of the invariant measure on this subspace, one can assign a probability p_i to every box and define the entropy:

$$H(\vec{s}, \delta) = -\Sigma_i p_i \ln p_i. \tag{4.41}$$

A second subspace $X_{\vec{t}}$ spanned by vectors $\vec{t}$ is then chosen such that $\vec{t} = \vec{F}(\vec{s})$, and therefore must be related to the dynamical constraints of the system. In this framework the joint probability p_{ij} for the system being in cell i of $X_{\vec{s}}$ and cell j of $X_{\vec{t}}$ is associated to the entropy,

$$H(\vec{t}, \vec{s}, \delta) = -\Sigma_{ij} p_{ij} \ln p_{ij}. \tag{4.42}$$

The conditional entropy

$$h(\vec{t}|\vec{s}, \delta) = H(\vec{t}, \vec{s}, \delta) - H(\vec{s}, \delta) \tag{4.43}$$

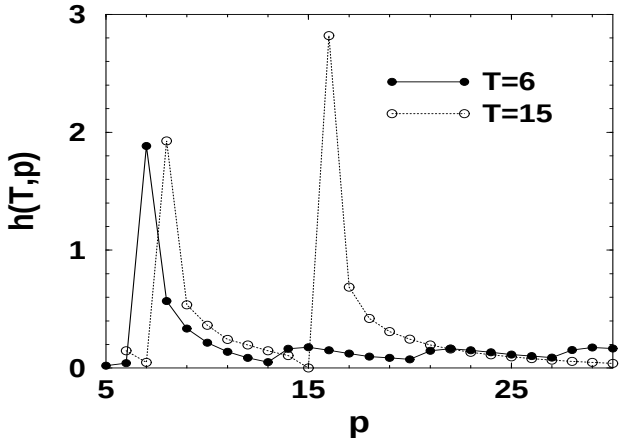

Figure 4.12: Convergence of estimates the topological entropy with finite values of period for $T = 6$ (solid line) and $T = 15$ (dashed line) for the Hénon map with $a = 1.0, b = 0.3$.

is independent of δ for δ small enough, in the the same as in section 4.2 the supremum over all partitions was replaced by a suitably fine partition.

In order to apply these ideas to the delayed maps, we define the subspaces mentioned above as:

$$\vec{s}_n = \{x_n, x_{n-T}\} \tag{4.44}$$

$$\vec{t}_n = \{x_{n+1}\}. \tag{4.45}$$

while conventionally one would choose $\vec{s}_n = \{x_n, x_{n-1}, ..., x_{n-T}\}$ but in the case of a scalar delayed map, the choice of (4.44) is more appropriate since $X_{\vec{s}}$ and $X_{\vec{t}}$ are related by a dynamical constraint. The conditional entropy given in Eq. (4.43) gives an upper bound for the metric entropy h_1 defined by Eq. (4.16). Better estimates of h_{KS} are based on a longer history:

$$h^m(\vec{t}|\vec{S}^{(m)}, \delta) = H(\vec{t}, \vec{S}^{(m)}, \delta) - H(\vec{S}^{(m)}, \delta) \tag{4.46}$$

with $m > 1$ and $\vec{S}^{(m)} = \{\vec{s}_n, \vec{s}_{n-1}, ..., \vec{s}_{n-m}\}$. And since we are using the Shannon entropy it is valid that:

$$h^1(\delta) \geqslant h^m(\delta) \qquad with \qquad m \geqslant 1 \tag{4.47}$$

In order to verify these ideas we have calculated the correlation entropy of time series generated by delayed maps. The choice of correlation entropy

instead of the Shannon entropy has practical reasons as explained at the end of section 4.2. Before we present the results of the correlation entropy two important points must be made: The inequality (4.47) does not hold for the correlation entropies (this can easily be seen from Eq. (4.8) with $\beta = 2$) and this entropy is a lower bound of the Shannon entropy, i.e. we cannot really expect to estimate upper bounds for the metric entropy. Keeping this in mind we proceed calculating the correlation entropy for some model systems.

First consider the Bernoulli map as in section 4.3.3. The correlation sum is calculated from Eq. (4.22) using state vectors constructed in the following way:

$$\vec{v}_n^{2m} = S^{(m)} \tag{4.48}$$

for even embedding dimension and

$$\vec{v}_n^{2m+1} = \{\vec{t}_n, \vec{S}^{(m)}\} \tag{4.49}$$

for odd embedding dimension. The corresponding results for correlation sum and dimension are shown in figure 4.13. Thus, with these state vectors, the correlation entropy that we are interested in (the counterparts of Eq. (4.46)) are given by

$$h_2(m, \delta) = \ln \frac{C_2(2m, \delta)}{C_2(2m+1, \delta)} \tag{4.50}$$

If m is large enough and in the limit of small δ, this entropy can be well recovered from the time series as shown in figure 4.14. In this example (using this embedding) the entropy can be recovered for $m = 1$ as long as δ is small enough (figure 4.14). The results shown in figures 4.13 and 4.14 show a surprising behavior: even without a saturation of the scaling with δ (leading to the embedding dependent dimensions), the entropy could be determined by comparing pairs of subspaces whose relation is completely deterministic.

The same ideas can be applied to estimate entropy of a continuous time delayed system but in this case two potential problems set in: The necessary discretisation and the mathematical definition (since phase space of delayed systems has infinite dimension cells to calculate the entropies have volume zero for any $\delta < 1.0$). The first problem is overcomed choosing a sampling intervals of equal but arbitrary length (of course the estimated entropy will depend on this length) and the second seems not to be an important one, as the dimension of the attractor is always finite [14]. In figure 4.15 the

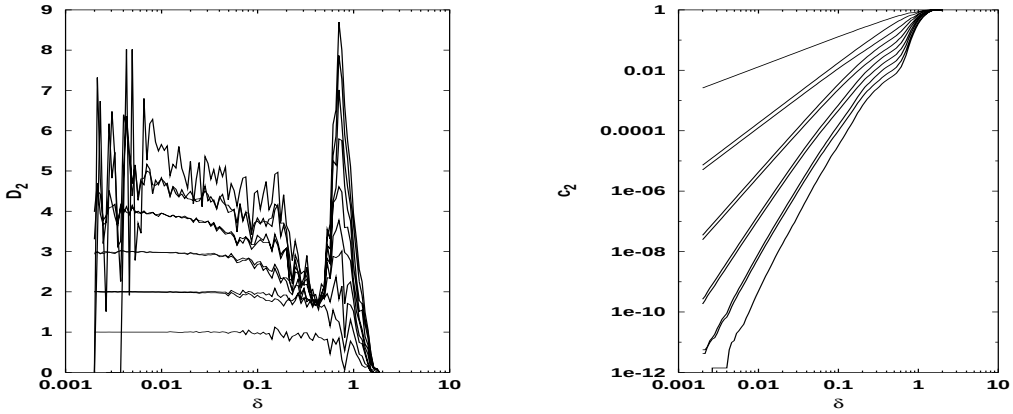

Figure 4.13: Correlation sum and correlation dimension for Bernoulli map with $T = 10$, $\epsilon = 0.3$ using a time series with $N = 10^9$ data points calculated using TISEAN package [2]. The slopes of the correlation sum are the correlation dimensions estimated with Eqs. (4.23). While the difference between two curves $2m + 1$ and $2m$ give the entropy of Eq. 4.50: Note that such difference tends to a definite value, even for small embedding dimensions, when the correlation dimension has not saturated.

correlation dimension and entropy of time series generated integrating the Mackey-Glass equation are shown. Also in this case, it was possible to obtain the entropy and to observe the same effect in the correlation dimension as in figure 4.13.

4.4.2 Metric entropies at large delay

The results presented in the former section, togehter with the existence of an asymptotic invariant measure on low dimensional projections of the phase space (see chapter 3) imply in an asymptotic value of metric entropy in the large delay limit. In fact, it is sufficient that the projection of the invariant density on the two dimensional space $x_n, x_{n-\tau}$ has an asymptotic form in the limit of large delay, in order that the upper bound obtained from Eq. (4.43) has an asymptotic value in this limit. We believe that this condition is fullfiled in general by delayed maps and present the behavior of the two point density $\rho(x_n, x_{n-\tau})$ of the Hénon map (see figure 4.16) as an example.

One could use the densities of figure 4.16 to obtain the estimate for the metric entropy using Eq. (4.43). However, by the same reasons and follow-

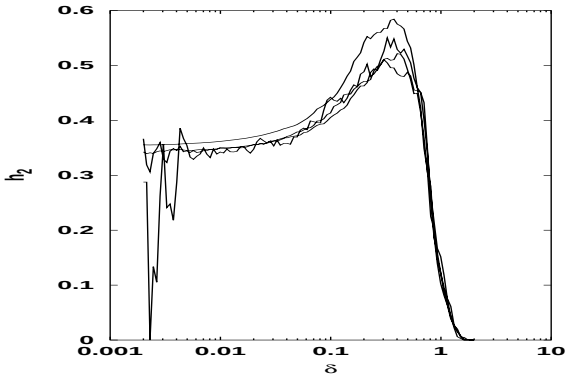

Figure 4.14: Estimating the correlation entropy for Bernoulli map using the same time series and the same procedure as in figure 4.13.

ing the same procedure as in the former section, we compute the correlation entropy for different delay values. The results shown in Fig. 4.17 demonstrate that in this case h_c^1 seems indeed to be a good upper bound for the metric entropy, and second that this entropy tends to an asymptotic value as the delay increases (as expected inspecting the densities in figure 4.16). In figure 1.2 it is possible to see how the value of the entropy flucutates around an asymptotic value: at low delay the fluctuations are larger since the measure has quite different properties at each delay value, at larger delay the fluctuations are smaller and related to the statistics in determining the Lyapunov exponents.

4.5 A simple stochastic process with delay.

The statistical description of dynamical systems provides a nice bridge between determinism and stochasticity. Until this point, we have only explored one side of this bridge, i.e. looked at determinstc dynamical systems with the toos developed to explore their statistical aspects. In this section, we will change the side for a while and investigate the entropy of a stochastic process with delay.

Entropies defined by (4.10) do not have a definite limit if the process has a continous phase space, they scale exponentially with $e^{-\delta}$. For us it is not very illuminating to investigate entropies of such processes and we focus on a process with a finite partition (with K elements), i.e. a Markov chain. We

define a special Markov chain fufilling the following property:

$$p(i_{m+1}|i_0, i_1, ..., i_m) = p(i_{m+1}|i_m, i_{m-T}). \tag{4.51}$$

and the condition probabilites do not change in time (stationary process). This "Markov chain with delay" is a simple stochastic counterpart of our delayed maps. To this process we can associate a transition matrix of dimension K^2 as in the case of two steps conventional Markov chains [44].

The process obeying Eq. (4.51) has some intersting features. First, having only the definition Eq. (4.51) it is not possible to calculate block entropies (4.14) for blocks shorter than $T+1$: All the entropies $p_j(m)$ must be specifiyed. Nevertheless, due to property (4.51) all the block entropies with $m > T+1$ are given by:

$$H_{T+k} = k \sum_{\omega(T+1)} p(i_0, i_1, ..., i_T) p(i_{T+1}|i_T, i_0) \ln p(i_{T+1}|i_T, i_0) + H_T \tag{4.52}$$

what follows from

$$p(i_0, i_1, ..., i_{T+k}) = \prod_{l=1}^{k} p(i_{T+l}|i_{T+l-1}, i_{l-1}) p(i_0, ..., i_T) \tag{4.53}$$

and from Eq.(4.14). Consequentelly, the KS entropy given by Eq. (4.16) is equal to

$$h_{KS} = \sum_{\omega(T+1)} p(i_0, ..., i_T) p(i_{T+1}|i_T, i_0) \ln p(i_{T+1}|i_T, i_0). \tag{4.54}$$

Hence, the entropy is not solely determined by the conditional probabilities $p(i_{T+1}|i_T, i_0)$ but all the probabilities $p(i_0, ..., i_T)$ must be known. In fact these probabilities are the invariant probabilities of sequences of length $T+1$ for the process under consideration and its value depends on the values of the transition probability. If the memory is longer, i.e. the future state does not depend only on one pair i_m, i_{m-T} but on q steps in the past such that:

$$p(i_{m+1}|i_0, ..., i_m) = p(i_{m+1}|i_m, i_{m-T}, ..., i_{m-q}, i_{m-T-q}). \tag{4.55}$$

The process is specifyed by a matrix of dimension K^{2q} [44] and the entropy is given by:

$$h_{KS} = \sum_{\omega(T+q)} p(i_0, ..., i_{T+q-1}) p(i_{T+q}|i_{T+q-1}, i_{q-1}, ..., i_T, i_0) \times \ln p(i_{T+q}|i_{T+q-1}, i_{q-1}, ..., i_T, i_0). \tag{4.56}$$

Thus, the longer the memory, the longer the sequence that must known in addition to Eq. (4.55) in order calculate the entropy.

As an example, let us consider that $p(i_0, ..., i_T) = 1/\omega(T)$, i.e. all sequences are equally probable. In this case the entropy of the chain of Eq. (4.51) is

$$h_{KS} = \sum_{i_0, i_T, i_{T+1}} \frac{\eta(i_0, i_T)}{\omega(T)} p(i_{T+1}|i_T, i_0) ln p(i_{T+1}|i_T, i_0). \tag{4.57}$$

where $\eta(i_0, i_T)$ is the number of sequences of length T such that the first symbol is i_0 and the last i_T. Since $\eta(i_0, i_T) \propto \omega(T)$ the entropy h_{KS} is independent from T and completelly determined by the transition probabilities, in this case.

We may ask what happens if the probabilities $p(i_0, ..., i_m)$ with $m \leqslant T$ are themselves defined through a one step Markov chain, e.g.

$$p(i_m|i_o, ..., i_{m-1}) = \tilde{p}(i_m|i_{m-1}) \tag{4.58}$$

with $m < T$. In this case, the KS entropy is given by:

$$h_{KS} = \sum_{i_0, i_T, i_{T+1}} \tilde{p}(i_0)\tilde{p}(i_T) p(i_{T+1}|i_T, i_0) \ln p(i_{T+1}|i_T, i_0). \tag{4.59}$$

what is expected due to the lack of correlation between symbols i_0 and i_T. Thus, as long as the marginal probability distributions $p(i)$ are fixed, the entropy is independent from the delay value. Similarly, $p(i_m|i_o, ..., i_{m-1}) = \tilde{p}(i_m|i_{m-1}, i_{m-2})$ it is possible to determine h_{KS} only with the knowledge of the two symbol probabilities $p(ij)$. And the same is true for q step process with $q < T$.

Defining a simpler process such that:

$$p(i_{m+1}|i_0, i_1, ..., i_{m-1}) = p(i_{m+1}|i_{m-T}). \tag{4.60}$$

one could think this is exactly a Markov chain of Eq. (4.58) with the time step equal to $T+1$ instead of 1. This is not the whole truth when sequences of symbols are to be considered and we end up with the same situation as in Eq. (4.51): In order to obtain the h_{KS} we need information about all sequences of length T, since

$$h_{KS} = \sum_{\omega(T+1)} p(i_0, ..., i_T) p(i_{T+1}|i_0) \ln p(i_{T+1}|i_0). \tag{4.61}$$

for Eq. (4.60). If $p(i_0, ..., i_T)$ are defined according Eq. (4.58) the KS entropy of (4.60) is given by:

$$\sum_{i_0, i_{T+1}} \tilde{p}(i_0) p(i_{T+1}|i_0) \ln p(i_{T+1}|i_0). \tag{4.62}$$

what corresponds exactly to the KS entropy of a conventional one step Markov chain.

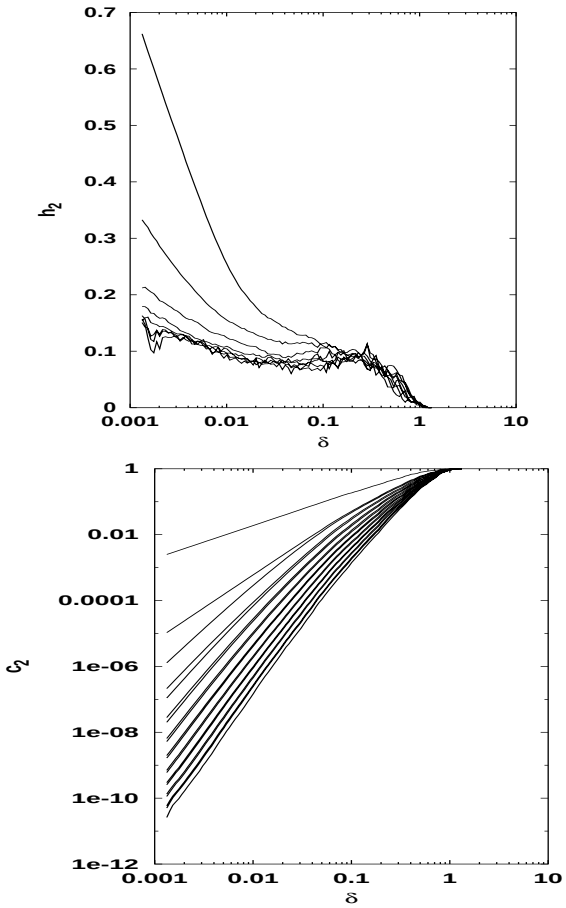

Figure 4.15: Correlation entropy and dimension for Mackey-Glass equation with $a = 0.2$,$b = 0.1$, $\tau = 50$. Samples are taken with a time interval $\tau/20.0$. The $h_{KS} = 0.09$ estimated from Pesin's identity.

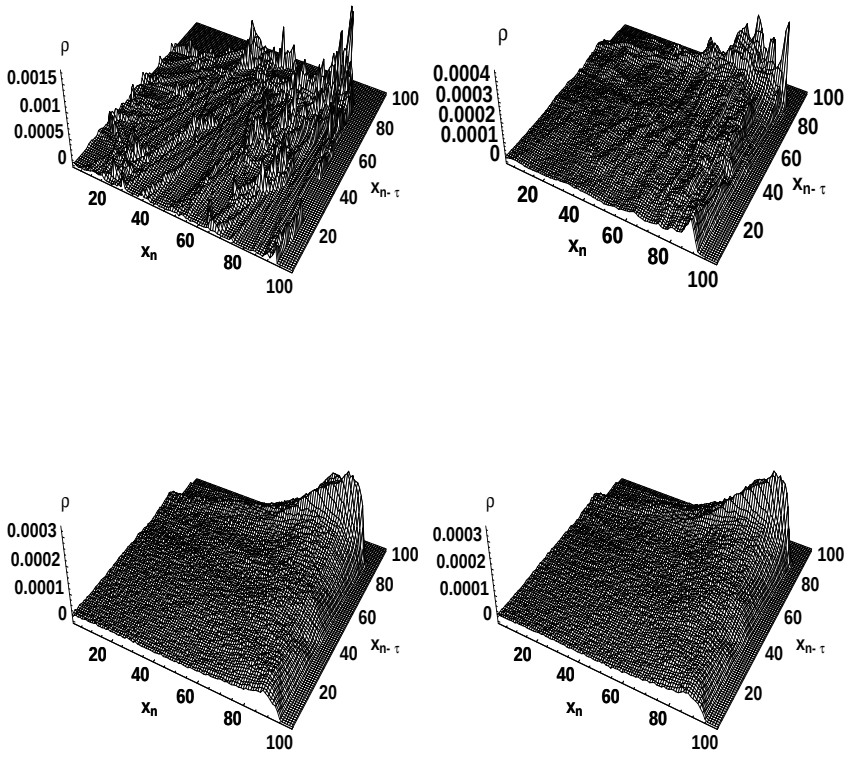

Figure 4.16: The two point density $\rho(x_n, x_{n-\tau})$ of the Hénon map with $T = 5, 10$ in the upper panel and $T = 20, 30$ in the lower panel . The densities are estimated from atime series with 10^7 points, partition the plane with a 100x100 grid of cells and calculating the relative frequency at each cell.

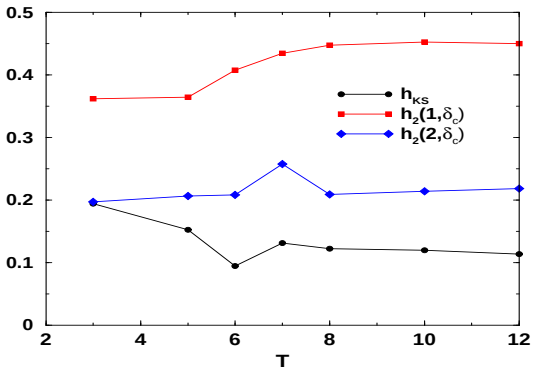

Figure 4.17: Correlation entropy estimated with $m = 1$ and $m = 2$ in Eq.(4.50) i.e. the counterpart of the Shannon entropy obtained with Eq.(4.43). And the KS entropy h_{KS} obtained from the Pesin's identity.

Chapter 5

Coupled map lattice from delayed maps

5.1 The representation

The idea of representing delayed differential equations of type Eq.(1.3) as spatially extended systems was firstly proposed by Ikeda and Matsumoto [45] by giving the time variable two different meanings: as a continuous variable θ bounded to a range of size τ, $\theta = t \bmod \tau$, and as an independent discrete variable n that counts how many delay units τ have run in the course of system evolution, $t = n\tau + \theta$. In this framework the delay-differential equation (1.3) is regarded as a discretized mapping rule from a spatial pattern at time n to a pattern at a time $n + 1$ (corresponding to an interval of τ in the real time). Later on, a similar representation was employed to organise data provided by an experimental system with delayed feedback, namely a single mode CO_2 laser [46], and it was observed that the trajectories in this representation produced patterns resembling those observed in real spatially extended systems. More recently, a more rigorous analysis has been carried out by introducing and computing the comoving Lyapunov exponents for a DDE and even deriving the amplitude equations for a suitable DDE near a Hopf bifurcation [11]. All known studies relating systems with delayed feedback to spatially extended systems consider only so called class-I systems as defined in [27] and hence all Lyapunov exponents scale like τ^{-1}. But also for class II DDE's (where the instantaneous dynamics itself is chaotic and hence at least one positive Lypaunov exponent does not scale with τ) it seems that the analogy is completely valid.

5.2 Error propagation : comoving Lyapunov exponents

In this section we will discuss the representation of delayed maps as coupled map lattices (CML) proposed in [27]. We show that the existence of an anomalous Lyapunov exponent in type II systems gives rise to infinite error propagation rates in the CML. The reason for this unphysical behaviour lies in the fact that the CML is unconventional in that it has an asynchronous, sequential updating rule in order to represent the delayed map. In order to eliminate the asynchronous updating we propose to represent the system in a rotated frame and discuss the dynamics in this frame.

We observe that in this case boundary conditions are crucial and we do not recover the original Lyapunov exponents. In each representation, the invariant density related to each site is the same, but the Lyapunov exponents and the comoving Lyapunov exponents are extremely dependent on the system representation.

For the sake of simplicity we will analyse a delayed map (DM) of the form:

$$x_{n+1} = (1-\varepsilon)F(x_n) + \varepsilon F(x_{n-T}) \tag{5.1}$$

where T is the delay time. We are interested in the thermodynamic limit, namely $T \to \infty$. This model contains all the phenomenology we want to discuss since through the parameter ε we can control the strength of the interactions of the delayed and instantaneous coupling, and hence it reproduces dynamics in all ranges from class-I to class-II maps as long as $f(x)$ is expanding, i.e. as long as the map $f(.)$ has chaotic dynamics.

In the representation of the system as a CML following [27] we have:

$$y_k^i = (1-\varepsilon)F(y_k^{i-1}) + \varepsilon F(y_{k-1}^i) \tag{5.2}$$

with the spatial index i and the temporal index k. The conversion rule from Eq.(5.1) to Eq.(5.2) is $i = n \bmod T$ (hence, $0 \leqslant i \leqslant T$), and $n = k(T+1)+i$, such that one time step of Eq.(5.2) corresponds to $T+1$ time steps of (5.1). The two representations are equivalent, if we impose "spiral" boundary conditions on Eq.(5.2), i.e., $x_k^{-1} = x_{k-1}^T$.

We have studied the propagation of disturbances on this lattice for the simple case of $F(x)$ given by Eq.(4.34) i.e. the Bernoulli shift. It is known from [27] that the corresponding delayed map has an anomalous exponent for $\varepsilon < 0.5$ (which will be a diverging quantity for the CML) while for $\varepsilon > 0.5$ all exponents scale like T^{-1}.

Concentrating on the spatial representation, we let the system evolve from a random initial condition until transients decay and introduce a disturbance at a site i_0 in a moment that we call $k = 0$. The disturbance u_k^i will evolve according to the following equation (and with the corresponding "spiral" boundary condition)

$$u_k^i = 2(1-\varepsilon)u_k^{i-1} + 2\varepsilon u_{k-1}^i \tag{5.3}$$

and after some time steps will spread over other sites different from i_0. In the case of $\varepsilon > 0.5$ the phenomenology resembles that of regular CML with unidirectional coupling: the perturbation evolves keeping an exponential profile in space while growing exponentially in time. For $\varepsilon < 0.5$ there is no well behaved profile. Instead, in a single time step, the disturbance will be spread over all sites and be macroscopic everywhere (for the large T we are interested in). In the thermodynamic limit ($T \to \infty$) the system turns a localised infinitesimal fluctuation into a global macroscopic event in one time step. See figure 5.1 for examples of both situations.

Propagation and growth of disturbances on a CML are well characterised by the comoving Lyapunov exponents [47], $\lambda(v)$, where $0 \leqslant v \leqslant T$ in our lattices. The definition is the following:

$$\lambda(v) = \lim_{k\to\infty} \log\left(\frac{|u_k^{[vk]}|}{|u_0^0|}\right) \tag{5.4}$$

where $[vk]$ denotes the integer part of vk. Analysing (5.3) one can see that in the interval $0 < \varepsilon < \frac{1}{2}$ there will be no error growth at zero velocity as $\lambda(0) = \log(2\varepsilon)$. However, propagation of disturbances with infinite velocity will take place as $\lambda(T) \approx T\log(2-2\varepsilon)$. Therefore, in the thermodynamic limit an unconventional kind of error propagation appears. In this range of $\varepsilon < \frac{1}{2}$ there is no correspondence between the comoving Lyapunov exponent at zero velocity and the conventional maximal Lyapunov exponent observed in a usual CML. Instead, the maximal Lyapunov exponent has the same value as $\lambda(T)$.

On the other hand in the interval $\frac{1}{2} < \varepsilon < 1.0$ there will be error growth at zero velocity and the value of the corresponding comoving Lyapunov exponent will be approximately equal to the maximal Lyapunov exponent of the system. The approximation will be better the nearer is ε to 1.0 or the larger the delay value is, i.e. in a range of parameters where the perturbation reentering through the boundary rule $u_{k+1}^{-1} = u_k^T$ is negligible. Under this

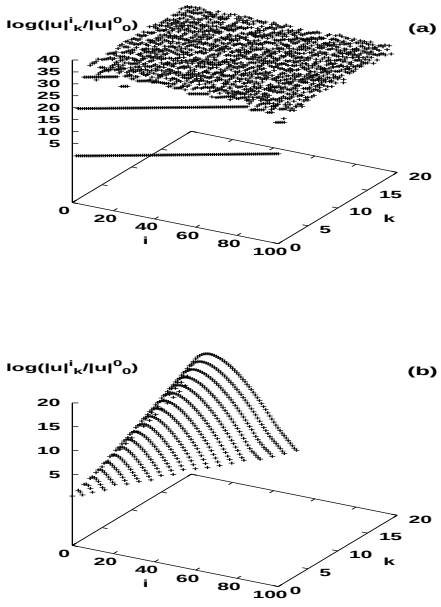

Figure 5.1: Propagation of disturbances in CML representations of a delayed map for $T = 100$. At $k = 0$ a disturbance $|u(0)| = 10^{-15}$ was introduced at site $i_0 = 0$. (a) $\varepsilon = 0.4$ (class II, one anomalous Lyapunov exponent), the disturbance becomes macroscopic after two time steps. (b) $\varepsilon = 0.8$ (class I), the disturbance grows smoothly and remains localised.

conditions, an initial perturbation of the form $u_0^i = \delta_{i,0}$ will evolve to the following form after k time steps:

$$u_k^i = C_k^i(2-2\epsilon)^i(2\epsilon)^k \tag{5.5}$$

where the coefficients C_k^i obey the recurrence rule:

$$C_k^i = C_k^{i-1} + C_{k-1}^i \tag{5.6}$$

with initial condition $C_0^i = \delta_{i=0}$ and boundary condition $C_k^{-1} = 0$ and Eq. (5.6) is then translated to

$$C_k^i = \Sigma_{j=1}^k C_j^{i-1} \tag{5.7}$$

from which one obtains the closed form for the coefficients:

$$C_k^i = \frac{1}{i!}\Pi_{j=0}^{i-1}(k+j) \tag{5.8}$$

Hence, using the definition (5.4) and the Stirling's formula we obtain the spectrum of comoving Lyapunov exponents of the map (5.3):

$$\lambda(v) = v\log(\frac{2(1-\epsilon)}{v}) + (v+1)\log(v+1) + \log(2\epsilon) \tag{5.9}$$

for $\varepsilon > \frac{1}{2}$ (see Fig. 5.2). These spectra display a nontrivial maximum, which corresponds to a nontrivial velocity of maximal amplification of disturbances (v_{max}), whose value obtained from Eq. (5.9) is given by:

$$v_{max} = \frac{2(1-\epsilon)}{2\epsilon - 1} \tag{5.10}$$

In Fig.5.3 we present numerical and analytical results for v_{max} as a function of ε. For $\varepsilon \to 1$, v_{max} approaches zero, and this is the only velocity at which amplification of disturbances takes place, i.e. the profile has zero width. As ε approaches the critical value of $\frac{1}{2}$, this velocity diverges, and we find the scenario described in the former paragraph.

The instantaneous spread of a localised infinitesimal perturbation and its infinite amplification factor $\approx T\log(2-2\varepsilon)$ with $T \to \infty$ is unphysical. It might have its explanation in the as well unphysical updating rule for the CML Eq.(5.2). This updating requires to run through one spatial layer sequentially (in order to know the value x_k^{i-1}), but at the same time assumes that this happens in a single time step. In order to gain a better

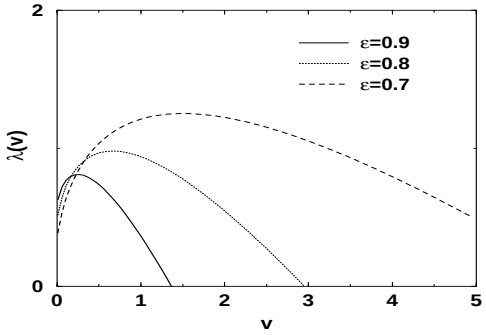

Figure 5.2: Spectra of comoving Lyapunov exponents calculated with Eq. (5.9).

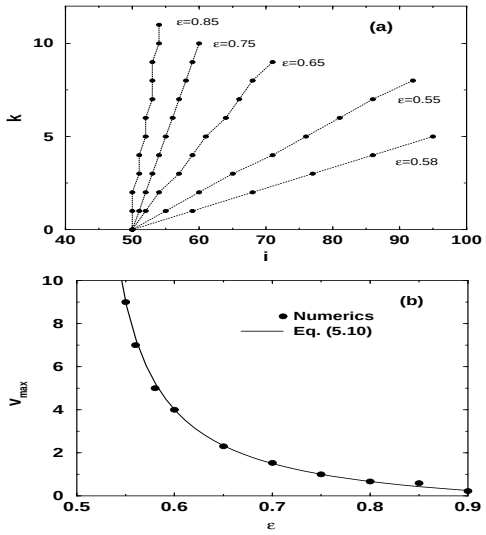

Figure 5.3: (a): Position i of the maximum of a disturbance profile after k time steps. The slope corresponds to v_{max}. (b): Velocity v_{max} of the maximal co-moving Lapunov exponent as a function of ε.

understanding, we have introduced a representation of the dynamics in a rotated frame as shown in figure 5.4. After rotation of the space-time axes by 45 degrees, we have two sub-lattices, where each two lattice sites on one sub-lattice uniquely determine the state at the enclosed site in the next sub-lattice. In order to arrive at a conventional CML, we consider the second iterate of the system, e.g., we focus on only the white sub-lattice of figure 5.4, where now every state is a function of three states in the past temporal layer. The dynamics is governed by a map of the form:

$$z_{k'}^{i'} = F(z_{k'-1}^{i'}, z_{k'-1}^{i'-1}, z_{k'-1}^{i'+1}) \tag{5.11}$$

In the case of the Bernoulli shift, disturbances evolve in this lattice according to the equation

$$u_{k'}^{i'} = 4(1-\varepsilon)^2 u_{k'-1}^{i'} + 8\varepsilon(1-\varepsilon)u_{k'-1}^{i'-1} + 4\varepsilon^2 u_{k'-1}^{i'+1} \tag{5.12}$$

and the comoving exponents behave exactly as in the case of a diffusive CML with asymmetric coupling. Therefore, we expect that in this representation, in the limit of $T \to \infty$ the existence of an anomalous exponent will not be related to infinite error growth. Indeed, if we repeat the study of disturbances already mentioned, we see that in the whole range of $0 \leqslant \varepsilon \leqslant 1$, disturbances propagate with a finite velocity. In figure 5.5 we depict how the velocity of maximal amplification depends on ε.

By analysing the spectrum of Lyapunov exponents in this representation (which coincides with the comoving Lyapunov exponents at zero velocity in this case) one can see that in the limits $\varepsilon = 0$ and $\varepsilon = 1.0$ the whole spectrum of Lyapunov exponents is negative (tends to $-\infty$) but there is propagation of disturbances at nonzero velocities ($v = +0.5$ and $v = -0.5$ respectively). At these velocities the maximal comoving Lyapunov exponent will be equal to $2\log(2)$. Therefore the system behaves like an open flow with convective instabilities where the perturbations will propagate and grow until they reach the boundaries and disappear. The growth rate is finite and independent from the chain length (for very long chains).

A first important conclusion at which we arise analysing the system is that the Lyapunov exponents seem not to be invariant under rotation of the space and time axes. The main reason for this lack of invariance lies in the modification of the boundary conditions: We have deliberately refrained from discussing them for Eq.(5.11). In fact, when the goal is to equip Eq.(5.11) with conditions such that its space-time pattern exactly reproduces the corresponding section of a space time pattern of Eq.(5.1),

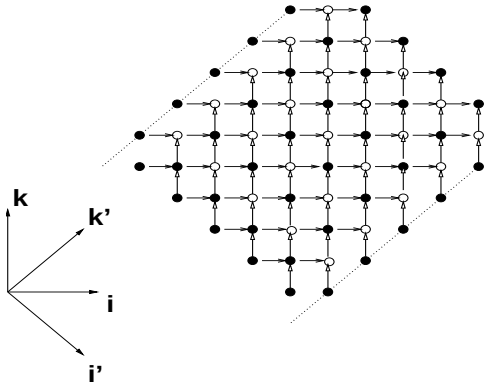

Figure 5.4: The representation of the DM as a CML in the 45^o rotated frame. The white circles represent the sites whose dynamics is governed by equation (5.11). Vertical/horizontal arrows correspond to the instantaneous and delayed coupling respectively.

these boundary conditions cannot be written in a simple closed form, but have to be copied from a full solution of Eq.(5.1). Any simple, closed form boundary condition for Eq.(5.11) is arbitrary and does not reproduce the details of the original dynamics. The surprising result here is that as long as $\varepsilon > \frac{1}{2}$, the two systems, Eq.(5.1) and Eq.(5.11), behave equivalently, whereas for $\varepsilon < \frac{1}{2}$ there is a dramatic difference. Of course, the explanation is not striking: The unphysical behaviour of Eq.(5.1) is generated by a combined effect of boundary condition and asynchronous updating rule. The error propagates and is amplified along a single spatial layer (this is the asynchronous updating) and is fed back through the left boundary after this huge amplification. In the rotated frame, this growth along a spatial layer corresponds to velocity 1/2 and creates hence a conventional exponential instability in time, and no re-insertion of an already huge error from the left exists.

Although at first sight this looks like a very particular situation in some rather artificial CML, it should serve as a warning that in spatially extended systems, an unphysical boundary condition can create unphysical effects even in the thermodynamic limit, where one would naively assume that boundary conditions are negligible.

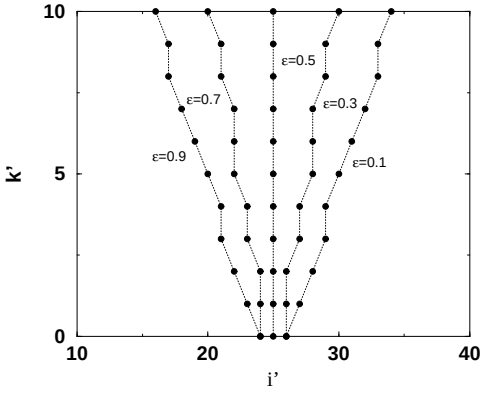

Figure 5.5: Dependency of the velocity of maximal propagation on ε in the rotated representation. In this plot $T = 100$, the dimension of lattice equal to 50 and the perturbation was introduced at the site $i_0 = 25$.

5.3 Time continuous case

The effect discussed above regarding the role of the anomalous exponent can be discussed also in the case of delayed differential equations (DDE). Following [11], we consider a simple linear DDE governing the dynamics of perturbations (e.g. near to a fixed point):

$$\dot{u}(t) = \mu u(t) + \eta u(t - \tau) \tag{5.13}$$

Using the same notation as in [11] the corresponding spatially extended system is given by:

$$\dot{u}(\sigma, \theta) = \mu u(\sigma, \theta) + \eta u(\sigma, \theta - 1) \tag{5.14}$$

Integrating Eq. (5.13) we find the following solution of this equation , with initial condition $u(\sigma, \theta) = \delta(\sigma)$:

$$u(\sigma, \theta) = e^{(\mu\sigma)} \sum_{i=1}^{\theta+1} \frac{C_i \eta^i e^{(\theta-i+1)\mu\tau} \sigma^{i-1}}{(i-1)!} \tag{5.15}$$

where C_i are some integer coefficients, that will be not be important here (its only worth to mention that $C_1 = C_\theta = 1$) . The solution given in [11]:

$$u(\sigma, \theta) = \frac{\eta^{(\theta+1)} e^{\mu\sigma} \sigma^\theta}{\theta!} \tag{5.16}$$

is recovered naturally when $\mu < 0$ in the limit of very large delay (or less naturally if one imposes that $u(\theta, \tau) = 0$ for any θ, i.e. one imposes fixed boundary condition). This would correspond to the case without an anomalous exponent.

When $\mu > 0$, the assumption of vanishing perturbation for $\sigma = \tau$ cannot be used, as exponentially growing perturbations appear just as in the case of maps and return to the system through the boundary. In the case $\mu > 0$ and $\eta << 1$ - this would correspond to $\varepsilon < 0.5$ in (5.3) - making the approximation $\eta^i \approx 0$ if $i > 1$ we get:

$$u(\sigma, \theta) = \eta e^{\mu(\sigma+\tau)} \tag{5.17}$$

and using the same definition of comoving Lyapunov exponents proposed in [11] we get:

$$\Lambda(\alpha) = \mu[\tau cos(\alpha) + \sin(\alpha)] \tag{5.18}$$

where $tan(\alpha) = \theta/\sigma$, and therefore $\alpha = 0$ will correspond to zero velocity. Hence, also in the case of DDE's one may find the unphysical error propagation discussed above in the case of large delay when the parameters value correspond to a regime where an anomalous Lyapunov exponent exists. The difference between this case and that of the maps is that here, one has finite growth rate at infinite velocity ($\Lambda(\pi/2) = \mu$).

5.4 Some conclusions

In summary we observed that in the most intuitive representation of a delayed map as a CML, the error propagation can happen with infinite rate when an anomalous exponent exists. This fact is associated with the asynchronous updating along with the boundary conditions. In the absence of such an exponent, however, all the phenomena observed in normal CML is recovered (perturbations decay exponentially in space and grow in time with a finite exponential rate). In a rotated reference frame, where the asynchronous updating is eliminated, the error propagation is physical. Indeed, in this rotated representation all comoving Lyapunov exponents are finite even in the presence of an anomalous exponent and in the cases $\varepsilon \approx 0$ or 1 the entropy of the rotated system will be zero if no entropy is introduced through the boundary. Beyond the results for DDE's, this serves as a warning that for spatially extended systems boundary 1conditions might influence strongly the behaviour of dynamical invariants even in the thermodynamic limit.

Chapter 6

Summary

The main conclusions of this work are the following:

1. Delayed differential equations of the form Eq.(1.3) and delayed maps of the form Eq.(1.4) have periodic orbits that reappear as the delay is varied. Such property is general and does not depend on the form of the map or differential equation. This property allowed us to study the stability of the orbits at different delays. In the case of maps an asymptotic form of the characteristic equation is obtained for orbits at different delay values which is related to an asymptotic form of the spectrum of Lyapunov exponents.

2. Low dimensional projections of the invariant density of delayed maps have an asymptotic form at large delay values. This fact is observed numerically. Some analytical treatment is performed up to first order in perturbation expansion for a map on a torus what shows that the convergence rate of the averages with the delay depends not only on the mixing rate of the instantaneous coupling but also on analytical properties of the function of the delayed coupling.

3. The topological entropy of delayed maps is bounded even in the limit of large delay. This fact can be observed from periodic orbits and their reappearance at different delay values. The estimates of the topological entropy from the orbits can only be obtained if the period is larger than the delay value.

4. An upper bound for the metric entropy can be obtained from the time series using a special embedding and this leads to the conclusion that

the asymptotic form of the low dimensional projection of invariant density is responsible for the asymptotic value of the metric entropies.

5. The representation of delayed maps or delayed differential equations as extended systems lead to unphysical error propagation rates when the system has an anomalous exponent.

Bibliography

[1] J-P. Eckmann and D. Ruelle. "Ergodic theory of chaos and strange attractors". *Rev. of Mod. Phys.*, 57:617, 1985.

[2] R. Hegger, H. Kantz, and T. Schreiber. "Practical implementation of nonlinear time series methods: The TISEAN package". *Chaos*, 9:413, 1999.

[3] R.D. Driver. *Ordinary and delay differential equations.* Springer, New York, 1976.

[4] S. Wiggins. *Introduction to applied nonlinear dynamical systems.* Springer, New York, 1990.

[5] E. Ott. *Dynamical Systems.* Cambridge University Press, Cambridge, 1993.

[6] M. C. Mackey and L. Glass. "Oscillation and chaos in physiological control systems ". *Science*, 197:287–289, 1977.

[7] J. Foss, A. Longtin, B. Mensour, and J. Milton. "Multistability and delayed recurrent loops". *Phys. Rev. Lett.*, 76:708, 1996.

[8] N. MacDonald. *Biological delay systems: linear stability theory.* Cambridge University Press, Cambridge, 1989.

[9] K. Ikeda and K. Matsumoto. "High-dimensional chaotic behavior in systems with time-delayed feedback". *Physica*, 29D:223–235, 1987.

[10] J. Simonet, E. Brun, and R. Badii. "Transition to chaos in a laser system with delayed feedback". *Phys. Rev. E*, 52:2294–2302, 1995.

[11] G. Giacomelli and A. Politi. "Relationship between delayed and spatially extended dynamical systems". *Phys. Rev. Lett.*, 76:2686–2689, 1996.

[12] M. Bestehorn, E.V. Grigorieva, H. Haken, and S.A. Kaschenko. "Order parameters for class-B lasers with a long time delayed feedback". *Physica D*, 145:110–129, 2000.

[13] M.C. Mackey. "Commodity price fluctuations and nonlinearities as explanatory factors". *J. Econ. Theory*, 48:497, 1989.

[14] J. Hale. *Theory of Functional Differential Equations*. Springer, Berlin, 1977.

[15] Z. Hong, L. Yaowen, W. Yinghai, and H. Bambi. "Dynamics in a system with time-delayed feedback". *Phys. Rev. E*, 58:4383–4390, 1998.

[16] R. Bellman and K.L. Cooke. *Differential-difference equations*. Academic Press, London, 1963.

[17] M.R. Roussel. "Approximating state-space manifolds which attract solutions of systems of delay-differential equations.". *J. of Chem. Phys.*, 109:8514–8521, 1998.

[18] H. Ueda, Y. abd Ohta and H. Bruce Stewart. "Bifurcations in a system described by a nonlinear differential equation with delay". *Chaos*, 4:1054–1500, 1994.

[19] W. Wischert, A. Wunderlin, A. Pelster, M Oliver, and J. Groslambert. "Delay-induced instabilities in nonlinear feedback systems". *Phys. Rev. E*, 49:203–219, 1994.

[20] J.D. Farmer. "Chaotic attractors of an infinite-dimensional dynamical system". *Physica*, 4D:366–393, 1982.

[21] P. Grassberger and I. Procaccia. "Measuring the strangeness of strange attractors". *Physica*, 9D:189–208, 1983.

[22] M. Le Berre, E. Ressayre, A. Tallet, H.M. Gibbs, D.L. Kaplan, and M.H. Rose. "Conjecture on the dimensions of chaotic attractors of delayed-feedback dynamical systems". *Phys. Rev. A.*, 35:4020–4022, 1987.

[23] J. Guckenheimer and P. Holmes. *Nonlinear Oscilations, Dynamical Systems and Bifurcations of Vector Fields*. Springer Verlag, New Yorke, 1983.

[24] D. Ruelle. *Thermodynamic formalism: the mathematical structures of classical equilibrium statistical mechanics*. Addison-Wesley, 1978.

[25] R. Artuso, E. Aurel, and P. Cvitanović. *Nonlinearity*, 3:325, 1991.

[26] M.E. Bleich and J.S.E. Socolar. Stability of periodic orbits controlled by time-delayed feedback. *Phys. Lett. A*, 210:87–94, 1996.

[27] S. Lepri, G. Giacomelli, A. Politi, and F.T. Arecchi. "High-dimensional chaos in delayed dynamical systems ". *Physica*, D70:234–249, 1993.

[28] O. Biham and Wenzel W. "Characterization of unstable periodic-orbits in unstable attractors and repellers". *Phys. Rev. Lett.*, 63:819, 1989.

[29] P. Grassberger, H. Kantz, and Moenig U. "On the symbolic dynamics of the Henon map". *J. Phys. A: Math. Gen.*, 22:5217, 1989.

[30] U. an der Heiden and M.C. Mackey. "The dynamics of production and destruction: analytic insight in complex behavior. ". *J. of Math. Biology*, 16:75–101, 1982.

[31] W. Just. "On the eigenvalue spectrum of time delayed Floquet problems". *Physica D*, 142:153–165, 2000.

[32] J. Losson and M.C. Mackey. "Coupled map lattices as models of deterministic and stochastic differential delay equations". *Phys. Rev. E*, 52(1):115, 1995.

[33] P Cvitanović, R. Artuso, R Marinieri, G Vattay, O. Biham, F. Christiannsen, and P. Dahlqvist. *Classical and Quantum Chaos. A cyclist threatise.* 2000. www.nbi.dk/ChaosBook/postscript.html.

[34] C. Beck and F. Schlogl. *Thermodynamics of Chaotic Systems - an Introduction*. Cambridge University Press, New Yorke, 1993.

[35] A. Lasota and M.C. Mackey. *Chaos, fractals and noise. Stochastic aspects of dynamics.* Springer, New York, 1994.

[36] T. Fisher and H. Rugh. *Erg. Th. of Dyn. Sys.*, 20:109, 2000.

[37] J.A. Yorke, P. Frederickson, J.L. Kaplan, and E.D. Yorke. "The Lyapunov dimension of strange attractors.". *J. Diff. Eq.*, 49:185–207, 1983.

[38] D. Ruelle. *Chaotic evolution of strange attractors.* Cambridge Univ. Press, Cabridge, 1990.

[39] P. Collet and J.P. Eckmann. *Iterated maps on the interval as dynamical systems.* Birkhäuser, Stuttgart, 1996.

[40] P. Walters. *An introduction to ergodic theory.* Springer, New York, 1982.

[41] C. Shannon. "A mathematical theory of communication". *The Bell System Tech. Journal*, 27:379, 1948.

[42] E. Olbrich and H. Kantz. "Inferring chaotic dynamics from time series: on which length scale determinism becomes visible". *Physics Lett. A*, 232:63, 1997.

[43] E. Olbrich, R. Hegger, and H. Kantz. "Local estimates for entropy densities in coupled map lattices". *Phys. Rev. Lett.*, 84:2132, 2000.

[44] D.R. Cox and H.H Miller. *The theory of stochastic processes.* Chapman and Hall, London, 1996.

[45] K. Ikeda and K. Matsumoto. . *Phys. Rev. Lett.*, 62:2265, 1989.

[46] F.T. Arecchi, G. Giacomelli, A. Lappucci, and R. Meucci. " ". *Physics Rev. A*, 45:R4225, 1992.

[47] R.J. Deissler and K. Kaneko. *Phys. Lett. A*, 119:397, 1987.

Acknowledgements

First of all, I am grateful to the support and encouragement of H. Kantz and W. Just who together supervised this thesis. I am also grateful to M. OrGuil for proposing and supervising together with H. Kantz a project about immunology.

I would like to thank the friends G. Corso, J. Engelmann, A. Langari, F. Langari, M. Ragwitz, U. Nitschke, M. Schulze, L. Matassini, A. Kaiser, H. Köllmer, and N. Baba for their kind hospitality and also M. Orguil for the help in a difficult moment. Moreover I am thankful to H. Emmerich and C. Faria for their attempts to help me with their advice.

This work was carried out with fellowship of DAAD whose financial support is gratefully aknowledged.